Geosci. Model Dev. Discuss., 8, 1945–2010, 2015
www.geosci-model-dev-discuss.net/8/1945/2015/
doi:10.5194/gmdd-8-1945-2015

Geoscientific Model Development Discussions
Open Access

MOPS-1.0: modelling the regulation of the global oceanic nitrogen budget by marine biogeochemical processes

I. Kriest and A. Oschlies

GEOMAR Helmholtz-Zentrum für Ozeanforschung Kiel, Düsternbrooker Weg 20, 24105 Kiel, Germany

Received: 27 November 2014 – Accepted: 2 February 2015 – Published: 24 February 2015

Correspondence to: I. Kriest (ikriest@geomar.de)

Published by Copernicus Publications on behalf of the European Geosciences Union.

Abstract

Global models of the oceanic nitrogen cycle are subject to many uncertainties, among them type and form of biogeochemical processes involved in the fixed nitrogen cycle, and the spatial and temporal scales, on which the global nitrogen budget is regulated. We investigate these aspects using a global model of ocean biogeochemistry, that explicitly considers phosphorus and nitrogen, including pelagic denitrification and nitrogen fixation as sink and source terms of fixed nitrogen, respectively. The model explores different parameterizations of organic matter sinking speed, oxidant affinity of oxic and suboxic remineralization, and regulation of nitrogen fixation by temperature and different stoichiometric ratios. Examination of the initial transient behaviour of different model setups initialized from observed tracer distributions reveal changes in simulated nitrogen inventories and fluxes particularly during the first centuries. Millennial timescales have to be resolved in order to bring all biogeochemical and physical processes into a dynamically consistent steady state, for which global patterns of biogeochemical tracers and fluxes are reproduced quite well. Analysis of global properties suggests that particularly particle sinking speed, but also the parameterization of denitrification determines the extent of oxygen minimum zones, global nitrogen fluxes, and hence the oceanic nitrogen inventory. However, the ways and directions, in which different parameterizations of particle sinking, nitrogen fixation and denitrification affect the global diagnostics, are different, suggesting that these may, in principle, be constrained independently from each other. Analysis of the model misfit suggests a particle flux profile close to the one suggested by Martin et al. (1987). Simulated pelagic denitrification best agrees with the lower values between 59 and 84 $\mathrm{Tg\,N\,yr^{-1}}$ recently estimated by other authors.

GMDD

8, 1945–2010, 2015

1 Introduction

The balance of "fixed", i.e. biotically available, nitrogen in the global ocean is determined by processes that either remove it (denitrification, anammox, burial) from, or add it (nitrogen fixation, atmospheric and riverine supply) to the ocean. The magnitude of these biotic and abiotic fluxes, and therefore the net balance of fixed nitrogen, is currently not well constrained. A decade ago, some geochemical and model-based studies suggested rather high fluxes (Codispoti et al., 2001; Gruber, 2004), sometimes with a high imbalance between sources and sinks (Codispoti, 2007), but more recent studies point towards lower, and balanced fluxes (Eugster and Gruber, 2012; DeVries et al., 2013; Somes et al., 2013), in accordance with earlier geochemical estimates (Gruber and Sarmiento, 1997).

Water-column denitrification and anammox are restricted to suboxic zones, i.e. regions with low oxygen, most notable the Arabian Sea, the Eastern Tropical North Pacific (ETNP) and the Eastern Tropical South Pacific (ETSP). Because nitrogen fixers experience their optimum growth in warm (surface) waters they are not generally expected to thrive in waters colder than 18 °C (Breitbarth and LaRoche, 2005; Breitbarth et al., 2007), and are therefore thought to be limited to low latitudes. So far, it is not entirely clear, whether areas of denitrification and nitrogen fixation are tightly coupled in space (Deutsch et al., 2007) or not (Landolfi et al., 2013). Some spatial decoupling could be deduced from the distribution of reported direct measurements of nitrogen fixation (Luo et al., 2012) and also from the temperature limitation of nitrogen fixers and generally cold surface waters associated with eastern boundary upwelling regions overlying regions of denitrification. In case of spatial segregation of nitrogen loss processes and nitrogen fixation, not only the processes themselves (and their representation in models), but also the feedback processes and the physical transport processes linking the respective regions are of importance. Relatively slow biogeochemical turnover rates may also be the reason for rather long residence times of nitrogen in the ocean, which

GMDD
8, 1945–2010, 2015

are estimated to range between ≈ 1000–4000 years (see Eugster and Gruber, 2012, and citations therein).

Attempts to further constrain the residence time of marine nitrogen will benefit from a better understanding of both the spatial relation of nitrogen loss processes and nitrogen fixation, and the individual biogeochemical processes themselves. For example, nitrogen loss processes are associated with, and sensitive to, low (and therefore difficult to measure) concentrations of organic substrates and oxidants. Direct incubation measurements have led to different interpretations of the relevance and magnitude of various processes that determine the loss of fixed nitrogen in different ocean regions (e.g. Kuypers et al., 2005; Ward et al., 2009; Bulow et al., 2010). A possible explanation for the apparent discrepancies is the dependence on substrate availability, which is difficult to conserve in incubation experiments (Ward et al., 2008; Galan et al., 2009; Kalvelage et al., 2013). Geochemical estimates based on nutrient ratios and/or the distribution of nitrogen isotopes, on the other hand, integrate over space and time, and therefore depend on our knowledge and assumptions of underlying physics.

Model-based studies, especially when combined with observations, may provide some insight into the associated processes, and help to integrate over space and time. As noted above, one of the two main drivers in setting the global budget and distribution of nitrogen is denitrification, a process confined to suboxic zones. Unfortunately, many models suffer from systematic deficiencies in the spatial representation of low oxygen areas, with often too large and too intense oxygen minimum zones (OMZs). Possible reasons include deficiencies in the description of diapycnal mixing (Duteil and Oschlies, 2011) and an insufficient representation of the equatorial current system and equatorial deep jets (Dietze and Loeptien, 2013). Applying strongly increased zonal isopycnal diffusivities in the equatorial current band, Getzlaff and Dietze (2013) could improve the performance of coarse-resolution models with respect to oxygen and temperature in the Eastern Equatorial Pacific. Duteil et al. (2014) recently showed that a very fine ($1/10^{\circ}$) spatial resolution can significantly improve the representation of the eastern

GMDD
8, 1945–2010, 2015

tropical Atlantic oxygen minimum zones by lateral ventilation via the better-resolved equatorial current system.

Another possible cause of model deficiencies is the representation of the sensitivity of nitrogen loss processes to ambient oxygen as a rather abrupt switch, that does not seem to match recent observations made in the Peruvian upwelling zone (Kalvelage et al., 2011). Given the long residence times of nitrogen mentioned above, model integration times of decades to centuries (e.g., experiments carried out by Moore and Doney, 2007; Landolfi et al., 2013) may not be sufficient to fully examine effects of different parameterizations of nitrogen fixation and/or denitrification and their mutual interactions and feedbacks mediated by oceanic transport and mixing processes.

A correct representation of nitrogen fluxes in global biogeochemical ocean models is challenging as it entails a large variety of spatial and temporal scales, from cell-scale biological–chemical interactions up to global circulation time and space scales. We here investigate the impact of different biogeochemical processes on the spatio-temporal coupling and magnitude of global nitrogen fluxes by means of global coupled biogeochemical models. In particular, we examine the sensitivity of nitrogen budgets to remineralization length scale, oxidant affinity of remineralization under oxic and sub-oxic conditions, temperature dependency and stoichiometry of nitrogen fixation. Benthic denitrification is not explicitly included in the current model that focuses on pelagic processes. Spinup times of the model experiments of several thousand years are sufficient to draw conclusions about feedbacks and the net impact of these processes on the global nitrogen distribution, budget, and fluxes. The paper is organized as follows: after an introduction into the model structure and experimental setup, we present some model results against the background of observed concentrations, inventories, and fluxes. We finally discuss some characteristic features of the model, that may shed some light on the dynamics of other model simulations as well as oceanic processes.

GMDD
8, 1945–2010, 2015

2 Model setup and experiments

The model simulates the cycling of phosphorus and nitrogen among nutrients (N), phytoplankton (P), zooplankton (Z), detritus (D) and dissolved organic matter (DOM), as described for the phosphorus cycle by Kriest et al. (2012). It further parameterizes burial of of organic matter (as phosphorus and associated elements) at the sea floor, and, to close the mass budget, its resupply via river runoff (Kriest and Oschlies, 2013). Hereafter, we refer to these model types as "CTL" (no burial) and "BUR" (burial at the sea floor). In Appendix A we present a brief overview over the P-based pelagic core of the model, which is common to CTL and BUR and refer the reader to Kriest et al. (2012) and Kriest and Oschlies (2013) for a detailed analysis of these models.

In these previous model versions, that contained the phosphorus but not the nitrogen cycle, remineralization of organic matter (i.e. organic phosphorus) back to inorganic nutrients (i.e. phosphate) continued even in the absence of oxygen, thereby parameterizing some form of "implicit denitrification" without explicitly accounting for other oxidants beside oxygen. In the model presented here, the inclusion of the nitrogen cycle allows for an explicit description of denitrification. Remineralization of organic matter now depends on the concentration of both oxygen and nitrate, which act as final electron acceptors for oxidation of organic matter. Remineralization ceases in the model once both oxidants have been reduced to very low levels. The stoichiometric balance of all organic substrates, products, and oxidants is parameterized following Paulmier et al. (2009). We here only briefly describe this Model of Oceanic Pelagic Stoichiometry (hereafter called "MOPS"), and refer to Appendix B for a detailed description.

2.1 Parameterization of remineralization and fixed nitrogen loss

In MOPS, nitrogen fluxes are coupled to phosphorus via fixed stoichiometric ratios. In particular, we prescribe the molar stoichiometric ratio of the nitrogen : phosphorus demand of the organisms, $d = 16$, and derive the oxygen demand of remineraliza-

GMDD
8, 1945–2010, 2015

tion, $R_{-O_2:P} = 170$ from d and implicit assumptions about other elemental ratios, as described in Paulmier et al. (2009, their Table 1).

Stoichiometric budget considerations suggest that on long time scales, and over large spatial areas both anaerobic ammonium oxidation and "canonical denitrification" (here: heterotrophic reduction of nitrate to dinitrogen) result in the same nitrogen loss, and are undistinguishable in the model context. We therefore refrain from resolving these processes explicitly, but refer to "denitrification" as oxidation of organic matter via reduction of nitrate to dinitrogen. The details and consequences of this alleged simplification, in light of recent observations, will be discussed below.

We assume that under suboxic conditions denitrification replaces aerobic remineralization with $R_{NO_3:P} = 0.8 \times R_{-O_2:P} - d$ as explained in Paulmier et al. (2009, their Table 1). The rate of fixed nitrogen removal ultimately depends on the availability of organic matter, nitrate, and the absence of oxygen. The parameterization of oxidant (nitrate, oxygen) affinity was inspired by observations made by Kalvelage et al. (2011), which suggest a more or less gradual decline of denitrification and anammox under increasing oxygen concentrations. In the standard model setup REF aerobic remineralization depends on the half-saturation constant (affinity) for oxygen uptake of $K_{O_2} = 8\,\mathrm{mmol\,O_2\,m^{-3}}$, while denitrification is inhibited by oxygen, and is further determined by a half-saturation constant for nitrate uptake, $K_{NO_3} = 32\,\mathrm{mmol\,N\,m^{-3}}$ (see Table 1), respectively. This value is at the upper end of experimentally derived estimates Jensen et al. (2009). A sensitivity experiment "DenHigh" investigates the model's response to a higher nitrate affinity of denitrifying bacteria, as represented by a lower half-saturation constant for nitrate ($K_{NO_3} = 8\,\mathrm{mmol\,N\,m^{-3}}$), while another experiment "RemHigh" examines the model's sensitivity to concomitant increase in nitrate and oxygen affinity of aerobic and anaerobic remineralization ($K_{NO_3} = 8\,\mathrm{mmol\,N\,m^{-3}}$ and $K_{O_2} = 2\,\mathrm{mmol\,O_2\,m^{-3}}$, together with a lower oxygen level for the onset of denitrification; see Table 1). Dependency on organic substrates (detritus, dissolved organic matter) is parameterized as a first-order process.

GMDD
8, 1945–2010, 2015

2.2 Parameterization of nitrogen fixation

The removal of fixed nitrogen via denitrification is counteracted by nitrogen fixation in the euphotic zone. In our model MOPS, this process depends on the availability of phosphate, the deviation of the ambient nitrate : phosphate ratio from a reference ratio d^*, and temperature. It is based on the observations by Breitbarth and LaRoche (2005) and relaxes the oceanic molar nitrate : phosphate ratio towards $d^* = 16$ with a maximum rate of $2\,\mathrm{nmol\,N\,L^{-1}\,d^{-1}}$ (see Table 1). Given the sparsity of observations of cyanobacteria biomass, we refrained from explicit simulation of cyanobacteria, and instead assumed zero net growth, with immediate release of fixed nitrogen as nitrate (which also assumes immediate nitrification in our model that does not resolve different inorganic nitrogen species). By assuming implicitly constant cyanobacteria biomass, and a relaxation of the nitrate : phosphate ratio via immediate release of fixed nitrogen, our approach is similar to the one described by Maier-Reimer et al. (2005) and Ilyina et al. (2013).

To account for uncertainties regarding parameterizations of nitrogen fixation, besides the reference model setup "REF" we present sensitivity experiments with a different stoichiometric target for simulated nitrogen fixation of $d^* = 14.28$ (the observed global average nitrate : phosphate ratio experiment "NFixStoich") and temperature-independent nitrogen fixation (experiment "NFixNoTemp").

2.3 Particle flux sensitivity studies

Previous model experiments have shown a great sensitivity of global tracer distributions to variations in the particle sinking speed (Kriest and Oschlies, 2008, 2013; Kriest et al., 2012). For all five model setups we thus carried out experiments with varying sinking speed. In terms of a particle flux profile given by $F(z) \propto z^{-b}$, where z is depth, these correspond to a variation of b between 0.6435 ("fast" sinking) over 0.858 ("medium") to 1.0725 ("slow" sinking) for all model experiments, and additionally to $b = 0.429$ ("very fast" sinking) and $b = 1.287$ ("very slow" sinking) for the reference setup REF.

GMDD
8, 1945–2010, 2015

2.4 Circulation model, spinup and initialization

Global model simulations were carried out using the "Tracer Transport Matrix" method described by Khatiwala (2007). We used a matrix derived from the "Estimating the Circulation and Climate of the Ocean" ("ECCO") project, which provides circulation fields that yield a best fit to hydrographic and remote sensing observations over a 10 year period, on a spatial grid of $1^\circ \times 1^\circ$ horizontal resolution with 23 vertical levels (Stammer et al., 2004). This transport matrix (more specifically: 12 monthly average matrices) was also applied by Kriest and Oschlies (2013), albeit with a different temporal resolution and spinup time (see below). Tests with the reference model and a shorter time step showed only little differences, particularly when compared to the impact of biogeochemical parameters.

The nitrogen cycle model MOPS presented here operates on many time scales, determined by the relatively fast biological surface processes, slower deep remineralization, and the global ocean circulation. In addition, if areas of fixed nitrogen gain and loss are spatially segregated, time scales of physical transport between these regions are of importance. To ensure full equilibration of all processes involved, we spun up the coupled system over 9000 years, using two time steps per day for tracer transport, and 16 time steps per day for the calculation of biogeochemical source-minus-sink terms (Kriest and Oschlies, 2013, used 1/8 d for tracer transport, and 1/64 d for biogeochemical processes, simulated over 3000 years). We initialized all experiments from observed distributions of phosphate, oxygen and nitrate (monthly mean values for January above 500 m, and annual mean values below), as provided by Garcia et al. (2006a, b). Initialization of other tracers has been carried out as in Kriest and Oschlies (2013). Given the long spinup time, the final tracer distribution of the model is independent of its initialization. This assertion is confirmed by a number of test simulations with very different initial biogeochemical tracer distributions with model setup REF with a spatial resolution and circulation as in Kriest et al. (2012). All tests with different initial spatial distributions of identical global phosphate inventory did always reach the

GMDD
8, 1945–2010, 2015

same steady state, even if the model was started from near zero oxygen and nitrate, indicating the robustness of the model results shown below.

Model simulations were mostly carried out on an SGI Altix ICE 8200 Linux cluster at the North-German Supercomputing Alliance (HLRN, www.hlrn.de), using different versions 3.x of PETSc (Portable, Extensible Toolkit for Scientific Computation, www.mcs.anl.gov/petsc/). We note that experiments on other hardware/platforms (e.g., Intel Sandybridge; CrayXC30) and with different versions of PETSc (up to version 3.5) resulted in very small – if any – differences in model results.

3 Results

3.1 Transient concentrations, inventories and fluxes

Figure 1 indicates that, depending on particle sinking speed, model spinup times of at least a few millennia are necessary in order to fully equilibrate the different processes in the model. Within the first few decades, all model setups started from observed tracer concentrations initially lose some oxygen. The loss continues for experiments with moderate or fast sinking speed, until oxygen approaches a global-average equilibrium value that is about 16 to 18 mmol O_2 m^{-3} lower than observed for the fast sinking scenario, and between 8 and 12 mmol O_2 m^{-3} lower for moderate sinking speed. Model experiments with slower sinking speed show a different transient response: after the initial decline of oxygen, global average oxygen content increases again, until it almost approaches its initial value (setup REF), or even exceeds it (setups DenHigh and RemHigh). Results of setup NFixStoich are very similar to those of REF, and not shown here.

A change in sign is also exhibited by the transient behavior of the globally averaged nitrate concentration in all "slow" scenarios of setups REF, NFixStoich, DenHigh, and RemHigh (Fig. 1). All model setups investigated exhibit an initial, very rapid loss of nitrate within the first few years (see also Fig. 2). This initial loss of nitrate can be at-

GMDD
8, 1945–2010, 2015

tributed to surface processes, converting the inorganic dissolved tracers into organic forms (dissolved and particulate organic matter) as can be deduced from the increase in total N found in almost all model configurations (Fig. 1). In addition to this process, the loss of nitrate by denitrification, and its supply via nitrogen fixation affects the inventory of this tracer on longer time scales. MOPS' nitrate inventory starts to increase within the first few centuries, until it finally approaches an equilibrium value which is slightly ("slow") or up to 2.5 mmol N m^{-3} ("fast") higher than at the beginning. An exception to this is experiment DenHigh, where, due to the higher nitrate affinity of denitrification, equilibrium nitrate in the slow sinking scenarios is slightly less than initially prescribed. Because in DenHigh more nitrate is used for oxidation, oxygen is higher than in setup REF.

Total fixed nitrogen is not affected by the above mentioned conversion of inorganic to organic nitrogen, therefore it lacks the initial rapid decline exhibited by the nitrate inventory (Fig. 1, lower panels). Total nitrogen first declines slightly in all "slow" model scenarios, except setup NFixNoTemp, which, due to the widespread occurrence of nitrogen fixation, may quickly compensate the loss through denitrification. After this initial decline, fixed nitrogen, like nitrate, equilibrates to values higher than initially prescribed – again with the exception of the "slow" scenario of model setup DenHigh.

Most important for the transient behaviour of fixed nitrogen are fluxes in the Eastern Tropical and Subtropical Pacific, as illustrated in Fig. 2. Phosphate averaged over two regions "EEP" (Eastern Equatorial Pacific, here: east of 140° W, ±10°) and "LLP" (low latitudes of the tropical and subtropical Pacific, ±40° latitude) shows only small initial variations (less then 0.1 mmol P m^{-3} variation all experiments; no figure). In contrast, nitrate in the EEP decreases strongly within the first few hundred years, most strongly for the slow sinking scenario, down to a deficit of 3.7 mmol N m^{-3}. Nitrate then approaches a minimum, first in scenario "fast" (around year 200). The slow sinking scenario takes much longer to reach that minimum (about 400 years). The initial decline of nitrate is subsequently followed by a slight increase during the next centuries in all scenarios. In the LLP, nitrate exhibits a far less pronounced transient, comparable

GMDD
8, 1945–2010, 2015

to that of phosphate. The different transients of both dissolved tracers phosphate and nitrate are mirrored in the nitrate : phosphate ratio, which shows a strong decline (by about 0.5–1 units) in the EEP within the first centuries, but only small variations in the LLP.

The strong variation of nitrate in the EEP is caused by vigorous denitrification, from initially ≈ 40 to ≈ 10–$50\,\mathrm{Tg\,N\,yr^{-1}}$ by year 900, while nitrogen fixation proceeds at a constant, low level of $< 10\,\mathrm{Tg\,N\,yr^{-1}}$. The difference between the two fluxes in this region results in a negative net flux of nitrogen. Despite this high net loss, fixed nitrogen in the EEP remains relatively constant after some centuries. This almost balanced fixed nitrogen budget, in the presence of high nitrogen loss, can be attributed to supply from the adjacent area LLP, which shows high nitrogen fixation, but relatively low denitrification. The resulting positive (between ≈ 10–$40\,\mathrm{Tg\,N\,yr^{-1}}$) net N flux into the LLP region matches the loss in the EEP. Thus, after the first millennium, the more or less stable fixed nitrogen inventories in both EEP and LLP regions can be explained by transport between the two regions, which each display local disequilibria between dominant N loss (EEP) and N gain (LLP). The interactions between these two regions are also reflected in the initial transient pattern of global fluxes, which more or less mirror the combined fluxes of both regions (see bottom panels of Fig. 2).

3.2 Steady state concentrations, inventories and fluxes

After the 9000 year spinup the final (near steady state) model solution is independent of its initialization, and solely reflects the combined effects of biogeochemistry and circulation. We can therefore use a comparison to observed tracers and fluxes in order to assess model skill and performance. In the next sections we first examine model fit against observations of dissolved inorganic tracers. Examination of nitrogen fluxes against the quite sparse observational data sets can provide a first insight into the adequacy of some model parameterizations. Comparison to more robust, bulk diagnostics helps to examine the general model behaviour. We finally combine some of the model-

GMDD
8, 1945–2010, 2015

data comparisons to a total, global misfit function, that should help to decide among the different model setups and scenarios.

3.2.1 Patterns of dissolved inorganic tracers

In steady state all models exhibit similar volume distributions of phosphate (see Fig. 3 for model setups CTL and REF; the other model setups show similar results, see Fig. S1 in the Supplement), which can be attributed to the fact that they are based on the same phosphorus "core". Variations in sinking speed play only a little role for the volume distribution of phosphate. Surprisingly, the models also show very little difference in the volume distribution of oxygen, which matches observations quite well particularly for the slow sinking scenarios. Even the introduction of the nitrogen cycle, together with oxidant-dependent remineralization, does not strongly affect the distribution of this tracer. Nitrate is simulated quite well by the slow sinking scenarios of model setups that explicitly include this tracer. The explicit simulation of nitrate results in an even better representation than nitrate diagnosed a posteriori from simulated phosphate times a constant stoichiometric ratio of 16. Replacing this ratio for conversion by the observed global mean ratio of 14.28 results in a better fit for all model experiments, yet this latter, empirically derived nitrate diagnostic provides only a weak constraint on model performance, because of its dependency on observations.

A common way to look at model performance with respect to observed tracers, is to combine information about simulated and observed SDs, correlation coefficient (R) and centered (unbiased) root-mean-square error (herafter referred to as RMSE$'$) in a so-called "Taylor"-plot (Taylor, 2001). Figure 4 shows these diagnostics for phosphate, oxygen, and nitrate of model setups CTL, BUR, and REF. Obviously, all models deteriorate with respect to phosphate with increasing sinking speed, as indicated by too high a SD, decreasing correlation coefficient, and RMSE$'$. However, differences for slow settling speeds are rather small. Likewise, except for extreme sinking velocities, model results are quite similar when examining the fit to observed oxygen. However, results are more variable (among model types, and with respect to different metrics) when

GMDD
8, 1945–2010, 2015

nitrate is considered, either diagnosed from phosphate times 16 for models CTL and BUR, or simulated explicitly for model REF. Firstly, for all model setups we find a quite strong overestimate of variance, and decrease in fit (RMSE and RMSE′) especially for fast sinking velocities. Further, model REF at first sight seems to exhibit a far worse fit to observations (with respect to correlation coefficient R and RMSE′) than BUR. This is in striking contrast to Fig. 3, which indicates a better fit of nitrate simulated by REF than nitrate diagnosed from BUR's phosphate. However, it is imortant to note that RMSE′ does not account for the bias in total nitrate concentration (see also Taylor, 2001; Jolliff et al., 2009). Therefore, although BUR matches the general pattern of nitrate distribution (via phosphate), its average concentration does not match the observed average of $\approx 31\,\mathrm{mmol\,NO_3\,m^{-3}}$, as indicated by its overestimate of volume $> 40\,\mathrm{mmol\,NO_3\,m^{-3}}$ (Fig. 3). As a result, model REF for each sinking speed shows a better fit to observations with respect to the total RMSE. In contrast to the normally used Taylor-plot RMSE′, which would favor model BUR over REF, the RMSE includes both the match to the pattern and to total tracer inventory, which are, in our case, best reproduced by model REF.

Despite the overall good match of the global distribution of dissolved tracers to observations, models may differ in regions which are particularly sensitive to the combined effects of oxygen supply, sinking and remineralization. For example, as shown above (Fig. 2), the eastern tropical Pacific seems to play a large role for of global fluxes, and thus global tracer inventories. To investigate this region further, in Fig. 5 we have a closer look at nutrients and oxygen averaged over ±5° in the eastern Pacific. The analysis is similar to the one presented in Dietze and Loeptien (2013), but integrates over the upper 6500 m, and thus disregards mismatches in the vertical distribution of tracers.

Simulated regional phosphate varies only slightly ($< 0.2\,\mathrm{mmol\,P\,m^{-3}}$) among the different model experiments. On the other hand, simulated nitrate shows large variations of up to almost $20\,\mathrm{mmol\,N\,m^{-3}}$ towards the American coast, much larger than would be expected from the variations in phosphate and some typical stoichiometry. Particularly

GMDD
8, 1945–2010, 2015

the slow sinking scenarios of all model setups that include nitrogen strongly underestimate observed nitrate. At the same time these model experiments are in quite good agreement with observed oxygen, especially when simulated with a high affinity of denitrification for nitrate. The fast-sinking model experiments that yield a somewhat better fit to observed equatorial nitrate content, however, systematically underestimate the equatorial oxygen inventory. Thus, all configurations of MOPS show mismatches for either oxygen or nitrate in this region, and no experiment is able to sufficiently represent both oxidants at the same time.

Diagnosing nitrate from phosphate in the phosphorus-only model BUR yields a quite good agreement to observations between 150 and 110° W when applying the global observed nitrate : phosphate ratio of 14.28. East of 110° W the model with slow sinking speed overestimates nitrate. Using a stoichiometric ratio of 16 as typical for marine phytoplankton composition (Anderson, 1995), and also typically used in numerical models, results in a strong overestimate of observed nitrate by model BUR over the entire transect. Hence, only with help of observed nutrient ratios this model agrees with observed nitrate, impeding the use of this tracer for model evaluation.

3.2.2 Patterns of fixed nitrogen sources and sinks

Simulated vertically integrated nitrogen fixation in steady state (year 9001) is $\leq 100\,\mu mol\,N\,m^{-2}\,d^{-1}$ for large parts of the subtropical ocean. Higher values of up to $200\,\mu mol\,N\,m^{-2}\,d^{-1}$ occur mostly in the Pacific, the western Atlantic Ocean, occasionally in the Caribbean Sea, and in the Arabian Sea and Bay of Bengal (Figs. 6 and 7). Depending on the parameterization of sinking speed and biogeochemistry, the central Pacific Ocean is characterized by large areas with fluxes $> 160\,\mu mol\,N\,m^{-2}\,d^{-1}$. Slow sinking speed, especially when combined with high nitrate affinity of denitrification (setup DenHigh) increases steady-state nitrogen fixation, which can be attributed to the compensation of an enhanced fixed nitrogen loss (Fig. 6; see also below). Simulated nitrogen fixation rates mostly lie well within the range of earlier estimates for the open ocean (e.g., Mahaffey et al., 2005; Staal et al., 2007; Kitajima et al., 2009). Note that the

GMDD
8, 1945–2010, 2015

model setups due to the here-employed maximum fixation rate of 2 µmol N m^{-2} d^{-1} cannot not reach some high values found by Kitajima et al. (2009) and Staal et al. (2007). The comprehensive data set by Luo et al. (2012, their Fig. 6a) shows enhanced integrated nitrogen fixation of ≈ 200–1000 µmol N m^{-2} d^{-1} in and near the Caribbean Sea, where our model experiments underestimate nitrogen fixation. Data coverage in the Pacific Ocean is less dense and shows values between ≈ 20–200 µmol N m^{-2} d^{-1}. This range is also covered by model simulations.

Because denitrification is restricted to regions with low oxygen, it is not as widely distributed as nitrogen fixation. Areas of simulated denitrification are the Arabian Sea and Bay of Bengal, the eastern tropical and subtropical Pacific extending north- and southwards to latitudes of about 30°, and the upwelling off Namibia and Angola (Figs. 6 and 7). The model experiments simulate highest vertically integrated rates in the latter two regions, where loss of fixed nitrogen can be as high as ≈ 10 mmol N m^{-2} d^{-1} (slow sinking scenario of model setup RemHigh). Because of the longer residence time of particles in midwater depths, simulated nitrogen loss increases with decreasing sinking speed. It further increases with nitrate affinity in setups DenHigh and RemHigh.

Maximum volumetric denitrification mirrors that of its vertical integral, and can be as high as 118 nmol L^{-1} d^{-1} (setup RemHigh with slow sinking). Highest modeled values occur in the eastern tropical and subtropical Pacific, followed by the upwelling off Namibia and Angola, and the Arabian Sea and Bay of Bengal, especially for slow sinking speed and/or high nitrate affinity. Simulated maximum values up to 43 nmol L^{-1} d^{-1} in the Arabian Sea/Bay of Bengal are higher than maximum observed rates of ≈ 25 nmol L^{-1} d^{-1} (Ward et al., 2009; Bulow et al., 2010), but most simulated values are in the range 2–20 nmol L^{-1} d^{-1}, and thus quite in agreement with the observations. High rates of nitrogen loss (up to ≈ 150 nmol L^{-1} d^{-1}) have been observed in the Benguela upwelling by Kuypers et al. (2005), and Kalvelage et al. (2011) even report values of almost 500 nmol L^{-1} d^{-1}. The model only simulates annual-mean rates up to 40 nmol L^{-1} d^{-1} in that region.

GMDD
8, 1945–2010, 2015

Off Chile and Peru maximum simulated rates of nitrogen loss range between ≈ 30–120 nmol L^{-1} d^{-1} which is within observed rates of fixed nitrogen loss (Hamersley et al., 2007; Galan et al., 2009; Kalvelage et al., 2011). However, most observations in this region are related to the anammox process, with little or no indication for denitrification off Peru or northern Chile. Some recent work suggests sporadic, yet very high rates of denitrification in this region (Dalsgaard et al., 2012). Comparison of our model results to these observations does not seem straightforward, as our model does not explicitly distinguish between different oxidation states of nitrogen, or between the mechanisms of fixed nitrogen loss. In the discussion section we will examine this alleged model deficiency, in light of the various observations made in this region.

3.2.3 Global fluxes and inventories

Particle sinking speed has a strong impact on the volume of OMZs. In models with slow sinking speed organic matter prevails in midwater depths for a long time, causing a strong depletion in oxygen due to remineralization, and thus a large suboxic volume (Fig. 8, left panel). If particles sink faster, they may be buried in the sediment before being remineralized – therefore, these model experiments exhibit the smallest suboxic volume. Increasing nitrate affinity (setup DenHigh) causes less depletion in oxygen, because more nitrate is used for oxidation of organic matter. Increasing both nitrate and oxygen affinity (setup RemHigh) increases the OMZ volume. The criterion for the definition of suboxia (here: $< 8\,\mathrm{mmol\,O_2\,m^{-3}}$ or $< 4\,\mathrm{mmol\,O_2\,m^{-3}}$) has a strong impact on the evaluation of model misfit: for the lower criterion, only fast sinking model experiments show a relatively good fit to observations, whereas for the higher criterion the "best" sinking speed depends on the parameterization of oxidant affinity (e.g., "slow" sinking for model setup DenHigh vs. "fast" sinking for model setup RemHigh). Thus, a model evaluation based on the suboxic volume can give very different results for different oxygen thresholds used to define suboxia (see also Gnanadesikan et al., 2013).

The effect of particle sinking on OMZ volume propagates into simulated global nitrogen fluxes. The larger suboxic volume of model scenarios with slow sinking speed

GMDD
8, 1945–2010, 2015

triggers high rates of denitrification (Fig. 8, middle panel). Moving to high nitrate affinity in setup DenHigh exhibits the highest global integrated nitrogen loss and balancing nitrogen fixation for any given sinking speed (see also Table 2). In contrast, in the scenario with "very fast" sinking of model setup REF no denitrification occurs, because of the lack of suboxic zones (see above). Turning off the temperature dependence of the model's diazotrophs that constrains nitrogen fixation to warm surface waters (setup NFixNoTemp) results in simulated fixed nitrogen gain in high latitudes, far away from suboxic regions of nitrogen loss (see also Fig. 7), and therefore increases globally integrated nitrogen fluxes. In steady state, global nitrogen loss and balancing nitrogen fixation increase by some 20 % with respect to experiment REF in sensitivity experiment RemHigh with higher oxidant affinity, and by 42 % when only nitrate affinity, but not oxygen affinity, is increased (setup DenHigh; see Table 2).

Because MOPS simulates pelagic denitrification as only nitrogen loss process, this loss has, in steady state, to be matched by nitrogen gain via nitrogen fixation. In the following paragraphs we will therefore focus mostly on pelagic denitrification and its comparison to other observed or simulated estimates. We refrain from a detailed comparison to global nitrogen fixation (which, in reality, and under the assumption of homeostasis, would have to balance benthic denitrification as well).

The overall magnitude of steady-state global integrals of pelagic nitrogen loss of 59–84 $\mathrm{Tg\,N\,yr^{-1}}$ diagnosed from our model simulations (Table 2 and Fig. 8) agrees roughly with the model estimates of Moore and Doney (2007), but is considerably lower than the 140 $\mathrm{Tg\,N\,yr^{-1}}$ simulated by Oschlies et al. (2008). The range of estimates of nitrogen loss based on observations is even larger: Codispoti (2007) suggested that water column denitrification should be even higher than 150 Tg per year, whereas substantially lower estimates of 52 to 81 Tg per year were obtained by Gruber and Sarmiento (1997), Galloway et al. (2004), Deutsch et al. (2004) and, more recently, Bianchi et al. (2012), Eugster and Gruber (2012), and DeVries et al. (2012, 2013).

Based on his high estimated nitrogen loss rates, Codispoti (2007) suggested that the, until then, generally lower estimates of oceanic nitrogen fixation might have been

GMDD
8, 1945–2010, 2015

too low. More recent estimates of nitrogen fixation are often higher (Deutsch et al., 2007; Eugster and Gruber, 2012, 130–175 Tg N yr^{-1}). Because our model MOPS does not include benthic denitrification, and because nitrogen fixation is parameterized to balance nitrogen loss, its global integral will necessarily be at the lower end of global estimates. For example, model results by Somes et al. (2013) point towards high rates of nitrogen fixation between 195–350 Tg N yr^{-1}, sufficient to balance combined pelagic and sedimentary nitrogen loss, the latter being about twice as high as the pelagic loss. Including benthic denitrification in MOPS would most likely increase the global nitrogen fluxes, but also result in a different dependency of these on particle sinking speed.

With global oceanic phosphorus being conserved in all model configurations, the simulated global nitrate : phosphate ratio depends on the variable global nitrogen inventory and hence on the simulated fixed nitrogen losses and gains, which in turn are sensitive to particle sinking velocities. The establishment of suboxic zones, and thus areas of enhanced denitrification, results in regions with a lowered nitrate : phosphate ratio (see also Fig. 2), finally with an effect on the the steady state global nitrate : phosphate ratio (Fig. 8 right panel). An extreme case is experiment REF with "very fast" sinking, in which no suboxia develops and consequently no denitrification occurs. In this case the assumptions implicit in the model description of nitrogen fixation, increase the global-ocean molar nitrate-to-phosphate ratio from its observed initial value of 14.28 to 16, the stoichiometric ratio for aerobic processes (Fig. 8, right panel).

The relation of higher nitrogen losses and gains corresponding to a lower global nitrogen inventory generally holds also between different model configurations, the exception being the sensitivity experiment NFixNoTemp with temperature-independent nitrogen fixation, which shows both higher denitrification and fixation and higher stoichiometric ratios when compared to the reference model setup REF. Generally, simulated global nitrate-to-phosphate ratios of the "slow" to "very slow" sinking scenarios are closest to the observed ratio. Thus, a high pelagic turnover of nitrogen in suboxic areas, as mediated via slow sinking or high affinity of denitrification towards nitrate,

GMDD
8, 1945–2010, 2015

pushes the simulated nitrate-to-phosphate ratio towards the observed ratio of global average nutrients.

3.2.4 A model metric based on concentrations and fluxes of phosphorus and nitrogen

So far, we have analysed the models' fit to different observed quantities separately. While most of the models discussed in this study fit spatial patterns of dissolved tracers about equally well, some differences arise for different particle sinking speeds. Also, as shown above (Fig. 4) and discussed by Jolliff et al. (2009), accounting for the model bias of non-conservative tracers such as nitrate may serve as an important additional information on model skill, and help to discriminate among the different model types. Investigating the fit to observed global inventories of non-conservative tracers, to OMZ volume, and to global pelagic nitrogen loss as a function of different model parameters further indicates some mutually independent controls exerted by the different global diagnostics (see Fig. 8).

In this subsection we examine to what extent these diagnostics can constrain individual process descriptions better than the standard metric of global distributions of phosphate and oxygen, pelagic and benthic fluxes of organic matter, and global oxygen inventory, applied previously to model BUR by Kriest and Oschlies (2013). Specifically, we add the spatial distribution of nitrate, the global nitrate inventory, and global pelagic nitrogen loss as three additional diagnostics. Individual observations of nitrogen fixation or nitrogen loss are not considered because of the sparsity of data sets, their bias towards certain regions, and differences between the model's intrinsic assumptions and observations (see above) that may complicate a direct comparison. Also not considered in our metric is the volume of suboxic regions, because of its pronounced sensitivity to the oxygen threshold used in the definition of suboxia (see above).

Most phosphorus-based metric components of our new model of the pelagic nitrogen cycle MOPS are similar to those for the phosphorus-only model BUR presented by Kriest and Oschlies (2013), i.e. we find the best fit for a model with a sinking speed

GMDD
8, 1945–2010, 2015

reduced relative to the classical Martin parameters. Similarly, in MOPS the global nitrate inventory is matched best for very slow sinking speeds (Fig. 9, lower left panel). Simulated global pelagic fixed nitrogen loss, on the other hand, shows a best fit to observations for model simulations with medium sinking speed (upper left panel of Fig. 9). Therefore, with the given weights of global integrated or average properties (see also Kriest and Oschlies, 2013) the overall misfit function now favours model experiments with a power law flux exponent of 0.858, as initially suggested by Martin et al. (1987). Unfortunately, it is not possible to distinguish among the different model setups REF, NFixNoTemp, NFixStoich and RemHigh, as all of them perform more or less equally well with respect to the combined metric. Thus, with a misfit function that gives equal weights to all types of observations, and for the parameter ranges investigated, the parameterization of oxidant affinity or nitrogen fixation may be less important for model performance than the parameterization of particle flux. It remains to be investigated whether this still holds if additional data e.g. for nitrogen fixation in the (currently unexplored) eastern tropical Pacific become available. It is encouraging, however, that MOPS, i.e. a model in which remineralization is confined to the oxic or nitrate-bearing regions, performs as good as model BUR with its assumed infinite supply of oxidants.

4 Discussion

In the above sections we have presented and evaluated a global ocean biogeochemical model, that applies oxidant-dependent remineralization in order to represent the pelagic cycling of phosphorus, oxygen, and nitrate. While model results show an – to our opinion – agreeable fit to observations, we nevertheless identified some critical characteristics of the model system, that may be of relevance for its performance, and also for the evaluation and skill assessment of other, similar model systems. These characteristics will be discussed below and include the transient model behaviour, the representation and constraints of remineralization under oxic and suboxic conditions,

GMDD
8, 1945–2010, 2015

and the close interplay of biogeochemical and physical components particularly in the eastern tropical Pacific.

4.1 Transient vs. steady state

Model results for the first few centuries after starting from observed initial biogeochemical tracer distributions indicate that mutual interactions between biogeochemical processes in the eastern equatorial Pacific and surrounding areas play a large role for model adjustment on a global scale. The adjustment time depends strongly on the assumed sinking speed of organic matter, indicating the need to individually test equilibration times for different biogeochemical setups. We note that, although patterns of tracer concentrations remain relatively robust after a few centuries, integrated global nitrogen gain and loss take up to millennia to finally level out at equal, and thus balancing, global rates. Our model simulations indicate substantial imbalances of fixed nitrogen sources and sinks over the first few hundred years after initialization with observed tracer concentrations in essentially all model runs, reaching some 10 to 20 $\mathrm{Tg\,N\,yr^{-1}}$ after 200 years (Fig. 2). This can be explained by the slow coupling between circulation, deep remineralization, and spatial separation of regions of fixed nitrogen loss and gain. Any deficiencies in the description of ocean transport or biogeochemical processes lead to strong initial changes in the nitrogen budget particularly in the eastern equatorial Pacific, where denitrification rates are high and small shifts in oxygen concentrations and/or biological production and subsequent export and remineralization can have a relatively large impact on local nitrogen fluxes. As seen in Fig. 2, these local changes are, in our model, to a large extent balanced by a response in nitrogen fixation in the surrounding regions of the tropical and subtropical Pacific. After 3000 years, we still find a gain of fixed nitrogen of 0.6–7.2 $\mathrm{Tg\,N\,yr^{-1}}$ (depending on particle sinking speed) for model setup REF (no figure), which then slowly declines to $< 0.4\,\mathrm{Tg\,N\,yr^{-1}}$ in year 9001 of the model scenario with very fast sinking speed; model experiments with slower sinking speed show a remaining imbalance $< 0.1\,\mathrm{Tg\,N\,yr^{-1}}$. Earlier model studies (Moore and Doney, 2007; Schmittner et al., 2008; Ilyina et al., 2013) with generally shorter

GMDD
8, 1945–2010, 2015

spin-up periods, reported imbalances between nitrogen fixation and denitrification of up to several $Tg\,N\,yr^{-1}$. According to our model results, this may be indicative of those models not having spun up for long enough to be in equilibrium. The above results indicate the need to spin up models over a long enough time in order to evaluate the full response of the coupled physico-biogeochemical system. Analysis of model results from shorter spinups may result in nitrogen fluxes, that reflect the transient, but not steady state characteristics of the system.

A number of test runs with altered nitrogen and oxygen initial conditions confirmed that the near steady state model solution reached after several thousand years (9000 years in our examples) is independent of its initialization (as long as the total phosphorus inventory is kept unchanged), and solely reflects the combined effects of biogeochemistry and circulation. Results from the nitrogen based model in steady state agree reasonably well with respect to observed tracer concentrations and fluxes, both with respect to local as well as to global quantities, giving some confidence in the model's representation of the large scale dynamics of marine nitrogen. The good match of the model MOPS that explicitly calculates nitrogen is promising, as this model agrees with observations even in the presence of more constraints (oxidant affinity of remineralization) than previous phosphorus-only model versions, that assumed an infinite supply of oxidants.

However, in steady state all model experiments exhibit some deficiency in nitrate or oxygen in the eastern equatorial Pacific, which may be either due to an ill-defined biogeochemical model, deficient representation of the physics, or both. For example, our model does not distinguish among the different oxidation states of nitrogen, it relies on rather weakly constrained parameters for oxidant affinity, and equatorial dynamics are notoriously difficult to represent by medium- to coarse-resolution ocean circulation models (Dietze and Loeptien, 2013). In the following subsections we will have a closer look at these model features, which should also provide some insight into the dynamics of models outside this study.

GMDD
8, 1945–2010, 2015

4.2 The importance of resolving different nitrogen species

As noted above, in some areas the model shows a quite good agreement to observed rates of denitrification. However, a direct comparison between simulated and observed rates of nitrogen loss is not always straightforward, as many observations refer to anammox, which is not explicitly resolved by the model. Further, some of the experiments measuring nitrogen loss have been carried out under high levels of nutrient additions, and may therefore be regarded as potential rates. For example, Kalvelage et al. (2011) found maximum anammox rates up to 108 $\mathrm{nmol\,L^{-1}\,d^{-1}}$ off Peru, but many rates were much lower. Potential anammox rates below 30 $\mathrm{nmol\,L^{-1}\,d^{-1}}$ have been observed by Galan et al. (2009), Hamersley et al. (2007) and Thamdrup et al. (2006). Most of these works found little or no indication for denitrification in the Pacific off Peru or northern Chile, but recent work by Dalsgaard et al. (2012) suggests sporadic, yet very high rates (up to 190 $\mathrm{nmol\,L^{-1}\,d^{-1}}$) of denitrification in this region, at that time much higher than the maximum observed anammox rate of 21 $\mathrm{nmol\,L^{-1}\,d^{-1}}$. Depending on the method of calculation, they arrived at a mean contribution of denitrification of 65–77 % to total mean removal of fixed nitrogen (2.1 $\mathrm{mmol\,N\,m^{-2}\,d^{-1}}$), which is in striking contrast to previous studies indicating a pronounced dominance of the anammox process (Hamersley et al., 2007; Thamdrup et al., 2006; Galan et al., 2009; Kalvelage et al., 2011). As suggested by Dalsgaard et al. (2012) a possible explanation for the very different contributions of denitrification and anammox found in the different studies could be the spatial patchiness of the relevant processes in this region.

In model MOPS presented here, we do not distinguish between denitrification and anammox, but assume only one process for the reduction of nitrate, "denitrification", where both steps of nitrogen reduction take place at the same rate, in conjunction with immediate, complete oxidation of ammonium released during both steps (as in Eqs. 13–18 of Paulmier et al., 2009). Given the controversy related to the importance of anammox and "canonical" denitrification on global and regional scales and the rather simplistic way, in which we implemented fixed nitrogen loss in the model, it seems

GMDD
8, 1945–2010, 2015

worthwhile to have a closer look at the model's intrinsic assumptions and their validity with respect to net nitrogen fluxes.

To examine the stoichiometric consequences of different pathways of fixed nitrogen loss, we first assume the complete denitrification pathway, i.e. complete oxidation of ammonium by nitrate, as suggested by Richards (1965), and applied by Paulmier et al. (2009, their Eq. 17). As an alternative pathway, we assume that ammonium released during the first step of denitrification is oxidized by anammox. As demonstrated in detail in Appendix C, with the assumed model stoichiometry both nitrogen loss pathways require 120 moles nitrate per 16 moles of ammonium (or one mole of organic phosphorus) oxidized. Thus, our current model stoichiometry can be regarded to represent either denitrification plus ammonium oxidation by nitrate, with both steps of denitrification proceeding at the same rate, or a combination of denitrification and anammox.

Note that in the absence of any nitrite accumulation, the combination of denitrification and anammox implies that the second step of denitrification happens 1.3 times faster than the first step (see Appendix C). In this case, the contribution of anammox to total dinitrogen production would only amount to $\approx 24\,\%$ (see also Fig. 11). If both steps of denitrification proceed at the same rate, we would again arrive at a low contribution of anammox of $\approx 26\,\%$. A contribution of 24–26 % for anammox is close to the values found by Dalsgaard et al. (2012), and discussed by Koeve and Kähler (2010) and Ward (2013), but is far lower than suggested by some observations made in the Peruvian upwelling region. A recent analysis confirms a rather low contribution of anammox, possibly depending on the carbon : nitrogen stoichiometry of organic matter, its oxidation state, and the magnitude of organic matter supply (Babbin et al., 2014).

Our simple theoretical framework suggests that anammox may, on average, only play a secondary role in determining the nitrogen loss in suboxic open-ocean areas. A more detailed model of different oxidation states of nitrogen, and other potential sources for ammonium, such as DNRA (see also the extensive analysis and discussion by Koeve and Kähler, 2010) or zooplankton excretion, would be required in order to investigate these processes in conjunction with diffusive transport processes across the oxycline

GMDD
8, 1945–2010, 2015

more closely. However, as shown above for biogeochemical tracer distributions simulated by a relatively coarse-resolution global model, it will not matter much whether the loss of fixed nitrogen is caused by denitrification or anammox, as both processes are ultimately fueled by organic matter and its remineralization products, with very small differences (or none at all) in the net stoichiometry and end products.

4.3 Constraints for oxidant affinity of suboxic processes

Motivated by the study by Kalvelage et al. (2011), we assumed for our model setups REF and DenHigh a wide tolerance of denitrification/anammox towards high levels of oxygen. However, recent studies by Dalsgaard et al. (2012) and De Brabandere et al. (2013) indicate that much lower oxygen concentrations are required for these processes to operate. The different observational estimates of oxygen thresholds of anammox were explained with regional differences among the study areas (De Brabandere et al., 2013). In an attempt to account for these uncertainties, we increased the oxygen affinity of aerobic remineralization and reduced the tolerance of denitrification to low oxygen in sensitivity experiment RemHigh.

In addition to uncertainties in the potential oxygen sensitivity of denitrifiers, their affinities to low nitrate concentrations are also not well constrained. For denitrifiers low half-saturation constants for the nitrate uptake during denitrification of 2.9 and 2.5 $\mathrm{mmol\,N\,m^{-3}}$ were measured in the Mariager Fjord in northern Denmark (Jensen et al., 2009) and in the Gotland Basin (Dalsgaard et al., 2013), respectively. However, direct comparison of these observed values to our model setup and results is complicated because of two reasons: firstly, environmental conditions in both studies were characterized by very low nitrite and low (usually $< 5\,\mathrm{mmol\,N\,m^{-3}}$) nitrate concentrations. Further, the electron donor for denitrification was usually sulfide instead of organic matter. These conditions differ from many open-ocean or even coastal-ocean environments considered here. Secondly, under addition of labelled nitrate, observed half-saturation constants were as high as 31 $\mathrm{mmol\,N\,m^{-3}}$ for nitrate reduction, and at least 15 $\mathrm{mmol\,N\,m^{-3}}$ for denitrification measured via addition of labelled nitrite (Jensen

GMDD
8, 1945–2010, 2015

et al., 2009), which has been explained with different substrate concentrations within and around the bacterial cells (Jensen et al., 2009). Given these methodological complications, and the regional differences between observations and our model setup, we are thus left with an uncertainty of an order of magnitude for the half-saturation constant for nitrate uptake during denitrification, ranging from 2.5 to 31 mmol N m^{-3}. This range of variation is to some extent addressed via our model experiments REF, DenHigh and RemHigh. It remains to be investigated, which half-saturation constant would be most appropriate for global simulations, and how far these would have to be changed when addressing more regional questions with more finely resolved models.

Although the effects of these parameters seem to be negligible for the overall, global volume distrution of dissolved tracers (Fig. 3), or for global metrics (Fig. 9), they influence the simulation of OMZ volume, global nitrogen flux and inventory (Fig. 8). Depending on questions posed to the model, it may therefore be important to constrain these parameters, either inversely, or via direct measurements particularly in open ocean areas of denitrification.

4.4 The representation of nitrate and oxygen in the eastern equatorial Pacific

Although some uncertainties in the paramaterization of nitrogen losses and gains remain, on long time scales model MOPS generally matches the global distribution of observed dissolved tracers and associated fluxes quite well. However, despite the quite different parameterizations of oxic and suboxic remineralization tested in this study, model experiments fail to represent all dissolved tracers simultaneously in the eastern equatorial Pacific (Fig. 5). The similar response of all model setups to changes in sinking speed suggests that processes other than than biogeochemistry – most likely, the physical exchange between the different regions, as suggested by Dietze and Loeptien (2013), play a role in determining the nitrogen budget in this region. Despite using circulation fields derived from a data-assimilative optimization of an ocean circulation model (Stammer et al., 2004), it is possible that our model circulation suffers from an imper-

GMDD
8, 1945–2010, 2015

fect representation of physical processes in this region, as has been hypothesized for many models by Dietze and Loeptien (2013).

So far, neither parameterization of oxidant-sensitivity, nitrogen fixation, or sinking speed has helped to relieve the models from these errors in the eastern equatorial Pacific (likewise, in the Arabian Sea or Bay of Bengal). Local increases of the zonal isopycnal diffusivity can help to emulate the yet unresolved Equatorial Intermediate Current System, and thereby improve the models (Getzlaff and Dietze, 2013). Given these possibly systematic model deficiencies, the spatial representation of suboxic zones and associated processes presented here must be viewed with caution. We hope, however, that the connection between areas of nitrogen fixation and nitrogen loss processes, and the associated transport timescales linking these regions in our model is representative of the real ocean.

4.5 Can we simulate and constrain the nitrogen cycle in a global biogeochemical model?

The above examples show that nitrate may, in models that explicitly account for denitrification, act as a kind of "scapegoat", that incurs the results of deficiencies built into the physical or biogeochemical model formerly represented by oxygen, or by unspecified oxidants. Nitrate diagnosed from simulated phosphate in model BUR is slightly less sensitive to variations in sinking speed (Figs. 3 and 5); however, its good fit to observed nitrate is only achieved with help of a strong dependency on observations. Given additionally the infinite supply of (undefined) oxidants embedded implicitly in model BUR, this "phosphorus-only" model may not be well suited to discriminate between the effects of biogeochemistry and physics on oxygen and other biogeochemical tracer distributions in this area. Therefore, the explicit simulation of the nitrogen cycle in global models may help to better constrain the dynamics of remineralization and its role in establishing and maintaining oxygen minimum zones.

Variation of parameters that govern remineralization, nitrogen fixation and denitrification can have quite different effects effects on properties such as the extension of

GMDD
8, 1945–2010, 2015

oxygen minimum zones, model nitrogen inventory, or global pelagic nitrogen fluxes. The different responses of these diagnostics to changes in either of these parameters are summarized in Fig. 10. Increasing particle sinking speed reduces the residence time of organic matter in the water column, thereby reducing aerobic remineralization, and the extent of OMZs. This then reduces global pelagic denitrification (because of a lower suboxic volume) and in steady state, the balancing nitrogen fixation. Because of a lower importance of denitrification at higher sinking speeds, and because of the prescribed stoichiometry of $N:P = 16$ under oxic conditions, the global nitrogen inventory increases. Increasing the nitrate affinity of denitrification reduces the size of the OMZ (because more nitrate, and less oxygen, is used for oxidation of organic material). However, the preference for nitrate also has the effect of increasing nitrogen fluxes, and thereby reducing the nitrate inventory. If additionally the affinity for oxygen is increased, both pathways (the aerobic and anaerobic remineralization) are enhanced, which to some extent cancels out any effect of global nitrogen fluxes and inventory. Relieving nitrogen fixation from its temperature constraint has the effect of increasing the nitrate inventory simply because of a more efficient compensation of nitrogen losses via denitrification. To sum up, the extent of OMZ, nitrogen fluxes and the nitrate inventory can be altered quite independently in the model, and therefore nitrogen and oxygen based diagnostics provide useful additional constraints for the model, as is illustrated in Fig 9. Together with the examination of the a priori assumptions of the model (see above subsections) we hope that in the future we will be able to make further progress towards a better constrained model of combined phosphorus, oxygen, and nitrogen cycles. However, depending on questions addressed with the model, one has to be careful in the choice of criterion for suboxia, and thus OMZ volume.

5 Conclusions

We have carried out model simulations using global coupled biogeochemical ocean models that simulate phosphorus, oxygen, and nitrogen fluxes. Starting from global

GMDD
8, 1945–2010, 2015

observed distributions of these tracers, our long term simulations indicate that model inventories and fluxes exhibit considerable changes within the first few decades to centuries, particularly in the eastern tropical Pacific, but also globally. Global integrated fixed nitrogen sources and sinks converge to a steady state only slowly, on millennial timescales, and suggest that that model results and trends achieved after spin-up periods shorter than a few thousand years should be viewed with caution.

Compared to a model without nitrogen cycle, but with some form of "implicit denitrification", dissolved nutrients and oxygen simulated by our new Model of Oceanic Pelagic Stoichiometry (MOPS) do not look very different, despite the fact, that the latter imposes many more functional controls on biogeochemical fluxes. Although in all models we can produce an equally good fit to observed nitrate by multiplication of simulated phosphate with the observed global stoichoimetric ratio, only the model with explicit nitrogen MOPS can predict this tracer prognostically, i.e. in the presence of more "mechanistic", a priori assumptions. For this model observations of nitrate, its inventory and global flux can serve as useful additional constraint.

In MOPS nitrate replaces oxygen as oxidant in certain regions. Especially in the eastern equatorial Pacific nitrate exhibits the mismatch that phosphorus-only models show with respect to observed oxygen distributions. In our model simulations the eastern equatorial Pacific plays a large role not only for the initial transient of the model, but also for steady state nitrogen fluxes. However, it is not clear how much of this response can be attributed to a deficient representation of the equatorial current system in this region.

Our model results are within the range of local, in-situ observations of nitrogen fixation and denitrification. So far, we have refrained from using local observations of nitrogen fixation for model calibration, the reason being a quite sparse data base, which exhibits a strong bias to certain oceanic regions (Luo et al., 2012). A closer examination of the effects of this bias on global and regional estimates, and the consequences or model calibration is beyond the scope of this study, and will be carried out elsewhere. As new data become available particularly in the so far neglected, yet sensitive eastern

GMDD
8, 1945–2010, 2015

tropical Pacific, these may provide very valuable benchmarks for model performance and skill.

Stoichiometric considerations indicate that for global models on relatively coarse spatial grids and simulated over long timescales it might not be necessary to differentiate between the various processes of fixed nitrogen loss, in particular denitrification and anammox. Correctly representing these processes is difficult without the explicit consideration of the various inorganic nitrogen species involved, and also depends on the availability of experimental data that determine and constrain the kinetics, substrates and oxidants of the different processes. A review of the few observations of oxidant affinities reveals a wide range of these parameters, indicating the need for further research, especially given the difficulty of the current model metric to constrain these from other observations. So far the sensitivity experiments with different remineralization kinetics have not revealed any dramatic changes in the simulated biogeochemical tracer distributions. On the other hand, experiments with different particle sinking speed indicate that not only the transient behaviour of the models depends on this parameter, but also the evolution of suboxic zones, and thus steady-state fluxes of fixed nitrogen (nitrogen fixation, pelagic denitrification), as well as the simulated global nitrogen inventory and the nitrate-to-phosphate ratio. However, this is probably partly due to the fact that in some model regions fast sinking organic matter quickly reaches the sediment, where it is ultimately buried. Considering benthic denitrification might shift this pattern, because in that case the oxidant deficiency at any given location cannot be neglected anymore.

With the given model setup, the effects of parameter variations on the extent of suboxic zones, nitrogen fluxes and inventories differ among the different parameters, and suggest to use these model diagnostics for model skill assessment. Including these new constraints in the overall misfit, our results point towards a “Martin” exponent of 0.86, and relatively low global fluxes of fixed nitrogen between 59–84 $\mathrm{Tg\,N\,yr^{-1}}$, the latter supporting more recent, observation-based estimates.

GMDD
8, 1945–2010, 2015

Appendix A: The biogeochemical phosphorus core

The core NPZD-DOP model simulates the cycling of phosphorus among nutrients (N, here: phosphate), phytoplankton (P), zooplankton (Z), detritus (D) and dissolved organic matter (DOP). The simulated phosphorus cycle has been described in detail in Kriest et al. (2012), therefore in the following we only summarize the main aspects of the model.

We assume that different biogeochemical processes operate in different vertical domains, with fast and dynamic turnover of phosphorus in the upper ocean layers, and a slow turnover of phosphorus below. To specify processes operating only in the euphotic zone (0–100 m, or $k \leq 6$), we use the symbol $H_e(k) \equiv H(k_e - k)$, where $H(k)$ is the Heaviside step function. $H_e(k)$ is "1" in the euphotic layers, and "0" outside.

A1 Euphotic zone

Phytoplankton (P) light limitation $f(I)$ is parameterized following Evans and Parslow (1985), using a globally uniform initial slope of the P-I curve of $0.025\,(\mathrm{W\,m^{-2}})^{-1}\,\mathrm{d}^{-1}$ (see also Kriest et al., 2010). Its maximum growth rate μ_{PHY} depends on temperature, with $\mu_{PHY}(T) = 0.6\,e^{\frac{T}{15.65}}$ (following Eppley, 1972, in the notation by Schmittner et al., 2008). We assume that the most limiting resource determines phytoplankton growth rate. Thus, phytoplankton growth is parameterized as $PP = \mu_{PHY}\,PHY_{min}(f(I), g(X_1, X_2, \ldots))$ where $g(X_1, X_2, \ldots)$ is a Monod function of only phosphate in models CTL andBUR, and a function of both phosphate and nitrate in MOPS (see Appendix B below). Phytoplankton experience a linear loss term of $\lambda_{PHY} = 0.03\,\mathrm{d}^{-1}$, and are grazed by zooplankton. Zooplankton grazing G is described by a Holling-III function, i.e. via a quadratic dependence on phytoplankton, a maximum grazing rate $\mu_{ZOO} = 2\,\mathrm{d}^{-1}$, and half-saturation constant $K_{ZOO} = 0.088\,\mathrm{mmol\,P\,m^{-3}}$. Only a fraction of grazing, $\epsilon_{ZOO} = 0.75$, is effectively ingested, the rest is released again via egestion. Zooplankton experience a quadratic mortality $\kappa = 3.2\,(\mathrm{mmol\,P\,m^{-3}})^{-1}\,\mathrm{d}^{-1}$. We assume that a fraction $\sigma_{DOP} = 0.15$

GMDD
8, 1945–2010, 2015

of egestion, zooplankton mortality, and phytoplankton loss is released as DOP, the rest becomes detritus. Zooplankton further experience a linear loss term of $\lambda_{ZOO} = 0.03\,d^{-1}$.

A2 All layers

DOP in all layers remineralizes with a constant rate $\lambda'_{DOP} = 0.17/360\,d^{-1}$, but only when present above a lower limit $P_{min} = 10^{-6}$ mmol P m^{-3}. In models CTL and BUR, remineralization continues even in the absence of oxygen, whereas in MOPS remineralization of DOP is a function of nitrate and phosphate (see Appendix B). Phytoplankton and zooplankton die with a constant mortality rate of $\lambda'_{PHY} = \lambda'_{ZOO} = 0.01\,d^{-1}$, again only when present above the lower concentration threshold P_{min}. The dead organisms immediately disintegrate to DOP.

Modelled detritus remineralizes with a fixed rate $\lambda'_{DET} = 0.05\,d^{-1}$ directly to phosphate. Again, in model MOPS its remineralization additionally depends on the availability of oxygen and nitrate (see Appendix B). We assume that the sinking speed of detritus increases linearly with depth, according to $w(z) = a\,z$, where z is the center of a layer. In steady state, and in the absence of any other processes, this parameterization can be regarded as equivalent to the so-called "Martin" (power law) curve of particle flux, with the exponent b given by $b = \lambda'_{DET}/a$ (see Kriest and Oschlies, 2008, for a detailed discussion). For easier comparison with other model studies, which explicitly define b, and for comparison with empirically observed values for this parameter, in our model experiments we prescribe b and evaluate a from it via $a = \lambda'_{DET}/b$. Note that in MOPS, due to reduction of remineralization by lack of oxidants, the local effective "Martin" exponent b may be smaller than initially prescribed.

A3 Oxygen and air–sea gas exchange

The air–sea gas exchange (top layer only) is parameterized following the OCMIP-2 protocol, with piston velocity and saturation computed from a monthly mean wind speed, temperature and salinity derived from the MIT ocean model, and interpolated linearly

GMDD
8, 1945–2010, 2015

onto the current time step. Oxygen also changes due to photosynthesis and remineralization, using a fixed stoichiometric ratio of $R_{-O_2:P} = 170\,\mathrm{mmol\,O_2/mmol\,P}$. While in earlier models, for $O_2 \geq 4\,\mathrm{mmol\,O_2\,m^{-3}}$ oxygen decreased proportionally to the concentration of organic matter, we now consider the dependence of remineralization on oxygen explicitly, as described on in Appendix B below.

A4 Benthic exchange

A fraction of detritus deposited at the sea floor (at the bottom of the deepest vertical box) is buried instantaneously in some hypothetical sediment. This loss, together with phosphorus budget closure via river runoff is described in detail in Kriest and Oschlies (2013).

A5 Source-minus-sink terms

The following equations describe the source-minus-sink terms for the earlier, phosphorus based models presented in Kriest et al. (2010), Kriest et al. (2012), and Kriest and Oschlies (2013). Changes due to the addition of the nitrogen cycle affect – as already mentioned above – phosphate (in particular: terms in Eq. A4), oxygen (Eq. A2), DOP (Eq. A7) and detritus (Eq. A13). These changes will be explained in detail in Appendix B.

$$\mathrm{S(O_2)} = R_{-O_2:P}\,(-\mathrm{PP} + \lambda_{\mathrm{ZOO}}\mathrm{ZOO})\,\mathcal{H}_e(k) \tag{A1}$$

$$+ R_{-O_2:P}\lambda'_{\mathrm{DOP}}\max(0, \mathrm{DOP} - P_{\min}) + R_{-O_2:P}\lambda'_{\mathrm{DET}}\mathrm{DET}^* \tag{A2}$$

$$\mathrm{S(PO_4)} = (-\mathrm{PP} + \lambda_{\mathrm{ZOO}}\mathrm{ZOO})\,\mathcal{H}_e(k) \tag{A3}$$

$$+ \lambda'_{\mathrm{DOP}}\max(0, \mathrm{DOP} - P_{\min}) + \lambda'_{\mathrm{DET}}\mathrm{DET}^* \tag{A4}$$

GMDD
8, 1945–2010, 2015

$$\mathrm{S(DOP)} = \sigma_{\mathrm{DOP}} \left[(1 - \epsilon_{\mathrm{ZOO}}) G + \kappa_{\mathrm{ZOO}} \mathrm{ZOO}^2 + \lambda_{\mathrm{PHY}} \mathrm{PHY} \right] \mathcal{H}_{\mathrm{e}}(k) \quad \text{(A5)}$$

$$+ \lambda'_{\mathrm{PHY}} \max(0, \mathrm{PHY} - P_{\mathrm{min}}) + \lambda'_{\mathrm{ZOO}} \max(0, \mathrm{ZOO} - P_{\mathrm{min}}) \quad \text{(A6)}$$

$$- \lambda'_{\mathrm{DOP}} \max(0, \mathrm{DOP} - P_{\mathrm{min}}) \quad \text{(A7)}$$

$$\mathrm{S(PHY)} = (\mathrm{PP} - G - \lambda_{\mathrm{PPHY}}) \mathcal{H}_{\mathrm{e}}(k) \quad \text{(A8)}$$

$$- \lambda'_{\mathrm{PHY}} \max(0, \mathrm{PHY} - P_{\mathrm{min}}) \quad \text{(A9)}$$

$$\mathrm{S(ZOO)} = \left(\epsilon_{\mathrm{ZOO}} G - \lambda_{\mathrm{ZOO}} \mathrm{ZOO} - \kappa_{\mathrm{ZOO}} \mathrm{ZOO}^2 \right) \mathcal{H}_{\mathrm{e}}(k) \quad \text{(A10)}$$

$$- \lambda'_{\mathrm{ZOO}} \max(0, \mathrm{ZOO} - P_{\mathrm{min}}) \quad \text{(A11)}$$

$$\mathrm{S(DET)} = (1 - \sigma_{\mathrm{DOP}}) \left[(1 - \epsilon_{\mathrm{ZOO}}) G + \kappa_{\mathrm{ZOO}} \mathrm{ZOO}^2 + \lambda_{\mathrm{PHY}} \mathrm{PHY} \right] \mathcal{H}_{\mathrm{e}}(k) \quad \text{(A12)}$$

$$- \lambda'_{\mathrm{DET}} \mathrm{DET}^* \quad \text{(A13)}$$

$$+ \frac{\partial w \mathrm{DET}^*}{\partial z}, \quad \text{with} \quad \mathrm{DET}^* = \max(0, \mathrm{DET} - \mathrm{DET}_{\mathrm{min}}) \quad \text{(A14)}$$

Appendix B: Coupling the nitrogen cycle to the phosphorus core

At this stage, we implement N in the simplest possible way, by considering only nitrate, but neither nitrite nor ammonium, as additional nutrient. Further, we assume that all biological components (i.e. phytoplankton, zooplankton, detritus and DOM) have a constant stoichiometry, given by $d = \mathrm{N} : \mathrm{P} = 16$. Thus, for the new, basic model "B" we only add one additional state variable to the phosphorus-based core model, namely nitrate. Adding nitrogen in this way requires the parameterization of three different processes: multiple nutrient limitation of phytoplankton growth, nitrogen fixation and heterotrophic nitrate reduction under suboxic conditions (hereafter loosely termed "denitrification").

GMDD
8, 1945–2010, 2015

B1 Multiple nutrient limitation

We assume a minimum function for the co-limitation of phytoplankton growth by phosphate and nitrate. First, we define the limiting nutrient L via

$$L = \min\left(PO_4, NO_3/d\right) \tag{B1}$$

If $L > 10^{-6}$, we then evaluate the combined light and nutrient limitation function in analogy to KKO12, i.e. we define total phytoplankton production as

$$PP = \mu_{PHY} PHY \min\left(f(I), \frac{L}{K_{PHY} + L}\right) \tag{B2}$$

where $\mu_{PHY}(T)$ and $f(I)$ are the maximum growth rate and light limitation as defined above, and $K_{PHY} = 0.03125\,\mathrm{mmol\,P\,m^{-3}}$ is the half saturation constant for nutrient uptake.

B2 Nitrogen fixation

Nitrogen fixation by marine diazotrophs supplies fixed N to the ocean. Unfortunately, sampling species such as *Trichodesmium* presents methodological difficulties (Breitbarth and LaRoche, 2005). E.g., assuming one *nifH* gene copy per cell results in calculated abundances up to $10^5\,\mathrm{cells\,L^{-1}}$ for station ALOHA near Hawaii (Goebel et al., 2007), corresponding to concentrations up to about $0.35\,\mathrm{mmol\,C\,m^{-3}}$. However, this is an order of magnitude higher than previous estimates from microscopic counts of *Trichodesmium* in this region (Letelier and Karl, 1996). Despite considerable recent efforts, global data sets for biomass remain relatively sparse, with only 2280 biomass estimates when gridded onto a $1^\circ \times 1^\circ$ grid with 33 vertical layers (Luo et al., 2012). Given the sparsity of observations, we thus refrained from explicit simulation of cyanobacterial biomass. Instead, we assume immediate release of fixed nitrogen as nitrate, resulting in a constant hypothetical population of diazotrophs, whose production rate equals the loss term.

GMDD
8, 1945–2010, 2015

We assume that nitrogen fixation in the model's euphotic layers depends on the nitrate : phosphate ratio and on temperature, T. Temperature dependence is parameterized based on observations of the diazotrophic filamenteous cyanobacterium *Trichodesmium*, which is responsible for a large fraction of global nitrogen fixation (Breitbarth et al., 2007). Instead of taking the fourth order polynomial fit of maximum growth rate to temperature presented in the study by Breitbarth et al. (2007), we have approximated their function for maximum growth by a second order polynomial, fitted over 20–34 °C. The resulting function has a maximum rate of 0.2395 d^{-1} at $T = 26.82$ °C. We then normalized the temperature dependent growth rate by the maximum rate. By doing so, we obtain a T-limitation curve that varies between 0 and 1 for a temperature range of 20–34 °C, and is zero elsewhere:

$$f_1(T) = \max\left(0, \frac{-0.0042T^2 + 0.2253T - 2.7819}{0.2395}\right) \quad \text{(B3)}$$

To examine the effect of temperature limitation, we carried out an experiment where we skipped the temperature dependency for nitrogen fixation (denoted as "NFixNoTemp"; see also Table 1 and below for more details).

Using a rather geochemical approaoch to restore fixed nitrogen towards the "Redfield" stoichiometry, we further assume that – in the presence of phosphate – nitrogen fixation is regulated by the nitrate : phosphate ratio:

$$f_2(N^*) = \max\left(0, 1 - \frac{NO_3}{d^* PO_4}\right) \qquad PO_4 > 10^{-6}. \quad \text{(B4)}$$

In the standard setup, nitrogen fixation relaxes the nutrient ratio to the stoichiometric relation used for the other biogeochemical processes, namely $d^* = d = 16$ (see Table 1). We further carried out an experiment "NFixStoich", where this process depends on the global observed nitrate : phosphate ratio, by setting $d^* = 14.28$.

Having defined the temperature and nutrient regulation of nitrogen fixation, both of which are allowed to vary between 0 and 1, we finally assign a rate of maximum

GMDD
8, 1945–2010, 2015

nitrogen uptake by cyanobacteria: under optimum conditions of $T = 26.82\,^{\circ}\mathrm{C}$ and nitrate $\ll$ phosphate, we set $\mu^{*}_{\mathrm{NFix}} = 2\,\mathrm{nmol\,N\,L^{-1}\,d^{-1}}$. This value is within the range of many observed rates: Oceanic rates usually range between 0 and $\approx 0.2\,\mathrm{nmol\,N\,L^{-1}\,h^{-1}}$, with some higher values up to $3.1\,\mathrm{nmol\,N\,L^{-1}\,h^{-1}}$ (Mulholland, 2007, we exclude one extremely high value from the Arafura Sea). The compilation by Staal et al. (2007, their Table 5) gives values between 0.07 to $17.3\,\mathrm{nmol\,N\,L^{-1}\,d^{-1}}$, with most values in the lower range. A value of $2\,\mathrm{nmol\,N\,L^{-1}\,d^{-1}}$ is also encompassed by the recent, comprehensive data compilation by Luo et al. (2012). However, in blooms or in certain incubations, rather high values were found (up to $30\,\mathrm{nmol\,N\,L^{-1}\,d^{-1}}$; Goebel et al., 2007; Staal et al., 2007; Kitajima et al., 2009). We thus consider our maximum value of $2\,\mathrm{nmol\,N\,L^{-1}\,d^{-1}}$ a more conservative estimate.

Note that combining our maximum uptake of $2\,\mathrm{nmol\,N\,L^{-1}\,d^{-1}}$ with the maximum normalized growth rate of $0.2395\ \mathrm{d^{-1}}$ implies a constant cyanobacteria concentration of $8.4\,\mathrm{nmol\,N\,L^{-1}}$, equivalent to about $0.05\,\mathrm{mmol\,C\,m^{-3}}$, when using a C : N ratio of 6.3. This concentration is lower than an estimate of $0.35\,\mathrm{mmol\,C\,m^{-3}}$ from *nifH* gene copies (Goebel et al., 2007), but close to the microscopic estimates of *Trichodesmium* cells (Letelier and Karl, 1996). The recent compilation by Luo et al. (2012) suggests very high biomass (up to $\approx 10\,\mathrm{mmol\,C\,m^{-3}}$) in the Caribbean Sea, and at the surface of the tropical Atlantic and the Arabian Sea. However, many open ocean values especially in the Pacific Ocean and/or deeper layers are rather low ($< 0.1\,\mathrm{mmol\,C\,m^{-3}}$). Thus, our implicit biomass estimates are in line with the observed estimates.

Choosing constant cyanobacteria concentrations, and the above mentioned dependence on nitrate : phosphate ratio we therefore follow a rather pragmatic approach, that parameterizes nitrogen fixation with immediate loss of fixed nitrogen to nitrate as antagonist to the fixed-N loss during denitrification (in $\mathrm{mmol\,N\,m^{-3}\,d^{-1}}$):

$$S^{\mathrm{NFix}}_{\mathrm{NO_3}} = \mu^{*}_{\mathrm{NFix}} f_1(T) f_2(N^{*}) \qquad \text{(B5)}$$

Note that nitrogen fixation with immediate remineralization of the fixed N to nitrate theoretically requires 1.25 mole oxygen = 2.5 oxygen atoms per mole nitrate produced.

GMDD
8, 1945–2010, 2015

So far, this is not included in the model, but from the analysis of several model simulations with the correct oxygen stoichiometry included for the simulated nitrogen fixation, we do not expect a large impact on model performance, as the oxygen fluxes in the euphotic zone will most likely be dominated by the air–sea flux.

B3 Remineralization under oxic and suboxic conditions

We do not distinguish between the different auto- and heterotrophic processes that may occur in suboxic regions, such as "canonical" denitrification, anammox, dissimilatory nitrate reduction, etc. Instead, in suboxic regions (here defined as regions where oxygen $< 40\,\mathrm{mmol\,O_2\,m^{-3}}$), we parameterize "denitrification" as anaerobic heterotrophic decomposition of organic matter, where nitrate as terminal electron acceptor is reduced to N_2. The implications and consequences of this assumption will be discussed below.

Motivated by recent observations of anammox and nitrate reduction under rather high (up to $25\,\mathrm{mmol\,O_2\,m^{-3}}$) ambient oxygen concentrations, and by the potential co-occurrence of both aerobic (ammonium oxidation) and anaerobic processes (Kalvelage et al., 2011), we parameterize a gradual increase of "denitrification" with decreasing oxygen concentrations. Firstly, we assume that maximum remineralization rates are the same for both aerobic and anaerobic processes, but that the sensitivities of these processes to oxygen and nitrate concentration are different. For a smooth transition between regimes of low and high oxidant concentrations we use a parameterization where the rate limitation depends on the square of oxygen concentration, i.e.,

$$I_{\mathrm{O_2}} = \frac{\mathrm{O_2^*} \times \mathrm{O_2^*}}{\mathrm{O_2^*} \times \mathrm{O_2^*} + K_{\mathrm{O_2}} \times K_{\mathrm{O_2}}} \tag{B6}$$

where we only consider oxygen above a certain threshold ($\mathrm{O_2^*} = \max(\mathrm{O_2} - \min_{\mathrm{O_2}}, 0)$). $\min_{\mathrm{O_2}} = 4$ and $K_{\mathrm{O_2}} = 8$ are the minimum concentration and half-saturation constant for the heterotroph's uptake of oxygen in setup REF, respectively. See Table 1 for values

GMDD
8, 1945–2010, 2015

of these parameters in the different experiments. To restrict oxygen consumption per time step, we first calculate the theoretical oxygen demand for respiration $u^T_{O_2}$:

$$u^T_{O_2} = l_{O_2}\left(\lambda'_{DET}\mathrm{DET}^* + \lambda'_{DOP}\mathrm{DOP}^*\right) R_{-O_2:P}\Delta t \tag{B7}$$

where $\lambda'_{DET} = 0.05\,[\mathrm{d}^{-1}]$ and $\lambda'_{DOP} = 0.17/360\,[\mathrm{d}^{-1}]$ are the remineralization rates of detritus and dissolved organic phosphorus, respectively, as defined above A. $\Delta t = 1/16$ is the time step length of the biogeochemical model in days. $R_{-O_2:P} = 170$ again denotes mole oxygen required per mole phosphorus remineralized (see Table 1). As in previous model versions, we restrict the minimum detritus and DOP concentration for the onset of remineralization: $\mathrm{DET}^* = \max(\mathrm{DET} - 10^{-6}, 0)$ and $\mathrm{DOP}^* = \max(\mathrm{DOP} - 10^{-6}, 0)$. The aerobic decay rate limitation is then

$$s_{O_2} = l_{O_2}\frac{\min\left({O_2}^*, u^T_{O_2}\right)}{u^T_{O_2}} \tag{B8}$$

If ${O_2}^*$ is lower than $36\,\mathrm{mmol\,O_2\,m^{-3}}$ additionally denitrification sets in. Again we define a quadratic rate limitation of this process, but reduce it by the inverse oxygen consumption rate:

$$l_{NO_3} = \frac{{NO_3}^* \times {NO_3}^*}{{NO_3}^* \times {NO_3}^* + K_{NO_3} \times K_{NO_3}} \times \left(1 - l_{O_2}\right) \tag{B9}$$

where ${NO_3}^* = \max(NO_3 - \min_{NO_3}, 0)$. $\min_{NO_3} = 4$ and $K_{NO_3} = 32\,\mathrm{mmol\,N\,m^{-3}}$ are the minimum concentration and half-saturation constant for the denitrifiers' uptake of nitrate in setup REF, respectively.

We note that the choice of the half-saturation constants of aerobic and anaerobic processes is rather arbitrary; however, as noted above the only gradual decrease of nitrate reduction (likewise for anammox) under increasing oxygen concentrations is

GMDD
8, 1945–2010, 2015

supported by observations. To account for the uncertainty especially in the nitrate sensitivity of denitrification, in setup "DenHigh" we decreased K_{NO_3} to 8 mmol N m^{-3}. In setup "RemHigh" we further evaluate the combined effect of high sensitvity of bacteria to both nitrate and oxygen by choosing the setup of "D" with a fourfold decrease of $\min_{O_2}$ and K_{O_2} (see also Table 1).

As for oxygen, we restrict the use of nitrate to the amount available:

$$u^T_{NO_3} = I_{NO_3}\left(\lambda_{DET}DET^* + \lambda_{DOP}DOP^*\right) R_{NO_3:P}\Delta t \tag{B10}$$

The rate limitation of anaerobic decay is then

$$s_{NO_3} = I_{NO_3}\frac{\min\left({NO_3}^*, u^T_{NO_3}\right)}{u^T_{NO_3}} \tag{B11}$$

Equation lines (A7) and (A13), which define the source-minus-sink terms due to remineralization of DOP and detritus, respectively, therefore change to

$$S^R_{DOP} = -\lambda'_{DOP}DOP^*\left(s_{O_2} + s_{NO_3}\right) \tag{B12}$$

$$S^R_{DET} = -\lambda'_{DET}DET^*\left(s_{O_2} + s_{NO_3}\right) \tag{B13}$$

Remineralization of DOP and detritus increases phosphate, thus changing Equation line (A4):

$$S^R_{PO_4} = +\left(S^R_{DET} + S^R_{DOP}\right) \tag{B14}$$

Likewise, Equation line (A2) for oxygen loss due to remineralization has to be replaced by:

$$S^R_{O_2} = -\left(\lambda'_{DET}DET^* + \lambda'_{DOP}DOP^*\right) s_{O_2} R_{-O_2:P} \tag{B15}$$

GMDD
8, 1945–2010, 2015

Aerobic decay of organic matter increases nitrate according to stoichiometric ratios. Under suboxic conditions, there is further a decrease of nitrate due to denitrification:

$$S^R_{NO_3} = \left(\lambda'_{DET}DET^* + \lambda'_{DOP}DOP^*\right) s_{O_2} d - \left(\lambda'_{DET}DET^* + \lambda'_{DOP}DOP^*\right) s_{NO_3} R_{NO_3:P} \quad \text{(B16)}$$

where $d = 16$ is the nitrogen : phosphorus ratio of organic matter as defined above, and $R_{NO_3:P} = 0.8R_{-O_2:P} - d = 120$ is the nitrate demand of remineralization of one mole phosphorus under suboxic conditions, as derived from the corresponding oxygen demand (see Paulmier et al., 2009, for stoichiometry of this process).

B4 Nitrate as a new state variable

Thus, considering additionally the change of nitrate due to biological processes in the euphotic zone, the time rate of change for nitrate is

$$S(NO_3) = d\,(-PP + \lambda_{ZOO}ZOO)\,\mathcal{H}_e(k) \quad \text{(B17)}$$

$$+ S^{NFix}_{NO_3} + S^R_{NO_3} \quad \text{(B18)}$$

Appendix C: Stoichiometry of denitrification and anammox

Consider 1 mole organic matter in phosphorus units (P_{org}), with the stoichiometric composition $C_aH_bO_cN_dP$. In our global model simulations we assume a composition of organic matter that requires 170 mole oxygen to oxidize one mole of organic phosphorus to carbon dioxide, water, phosphate, and nitrate. This value has been derived from geochemical observations (Anderson and Sarmiento, 1994), and has been applied in global biogeochemical models (e.g. Najjar et al., 2007; Moore and Doney, 2007). With $d = 16$, we define the oxygen demand for oxidation of organic matter to carbon dioxide,

GMDD
8, 1945–2010, 2015

water, phosphate, and ammonium via $R_0 = 170 - 2d = 138$ (see also Paulmier et al., 2009).

Under suboxic conditions, we first assume complete oxidation of ammonium by nitrate, as suggested by Richards (1965). Table 1 of Paulmier et al. (2009) indicates that for $R_0 = 138$ oxidation of one mole organic phosphorus requires $4/5R_0 + 3/5d = 120$ moles nitrate, which is reduced completely to dinitrogen, without any surplus of nitrite.

In an alternative approach we now consider anammox for oxidation of the ammonium released during suboxic degradation of organic matter, and assume that assume that nitrite reduction during denitrification takes place at a rate x of nitrate reduction. We then arrive at the following, bulk stoichiometry for complete remineralization of 1 mole organic phosphorus:

$$1\mathrm{P_{org}} + \frac{2R_0}{1+x}\mathrm{HNO_3} \rightarrow \left(\frac{2-\frac{4}{3}x}{1+x}R_0 - d\right)\mathrm{HNO_2} + \left(\frac{\frac{2}{3}x}{1+x}R_0 + d\right)\mathrm{N_2} + \{\ldots\} \qquad \text{(C1)}$$

Case $x = 0$, i.e. no nitrite reduction via denitrification, results in a considerable surplus of nitrite ($2R_0 - d = 260$ mole nitrite for each mole of organic phosphorus remineralized), even though anammox consumes some of it (see Fig. 11a). Even for $x = 1$ with the given stoichiometry 30 moles nitrite would be generated per mole of remineralized organic phosphorus. The surplus of nitrite appears because during nitrate reduction the ratio of ammonium released from organic matter to nitrite produced from reduction of nitrate is not 1 : 1, as required for anammox. Only for $x = (2R_0 - d)/(4/3R_0 + d) = 260/200 = 1.3$ no "left-over" nitrite would accumulate on the right hand side of equation C1. In this case, oxidation of one mole of organic phosphorus requires $4/5R_0 + 3/5d = 120$ mole nitrate.

To summarize, with the assumed model stoichiometry, and in the absence of any nitrite or ammonium accumulation, both cases require 120 mole nitrate per 16 moles of ammonium oxidized, i.e., our current model stoichiometry can be regarded to represent either denitrification plus ammonium oxidation by nitrate (with both steps of denitrification proceeding at the same rate) or a combination of denitrification and anammox. The

GMDD
8, 1945–2010, 2015

latter case implies that the second step of denitrification happens 1.3 times faster than the first step, to avoid any nitrite accumulation.

Unfortunately, very little is known regarding the contribution of the different processes to nitrogen cycling in suboxic waters. Investigations in a Danish fjord rather suggest a dominance of nitrate reduction over nitrite reduction (Jensen et al., 2009) which, in our theoretical framework, would correspond to $x < 1$. However, given the quite unique hydrographical and biogeochemical conditions of that study (low nitrate and nitrite, sulfide as electron donor) it is not clear whether these findings can be transferred to our study, which focuses on the open ocean.

Assuming no nitrite reduction by denitrifiers at all ($x = 0$) would result in a contribution of anammox of 100 %, but would also result in a large surplus of nitrite, which does not seem to agree with observations. In the case $x = 1.3$ (no leftover nitrite), the contribution of anammox to total dinitrogen production would only amount to ≈ 24 % (see also Fig. 11). If both steps of denitrification proceed at the same rate ($x = 1$), we would again arrive at a low contribution of anammox of ≈ 26 %.

Appendix D: MOPS-1.0 biogeochemical subroutines

The biogeochemical subroutines have been coupled to the "Transport Matrix Method" (Khatiwala et al., 2005). That source code, forcing, etc. together with an earlier version of this model, is available under https://github.com/samarkhatiwala/tmm. We here only briefly describe the different biogeochemical subroutines, and refer the reader to that website, and to the documentation in the Supplement that accompanies this manuscript.

The code mainly consists of "outer" routines (`external_forcing_kiel_biogeochem.c`, `kiel_biogeochem_ini.F`, `kiel_biogeochem_model.F`), that connect to the TMM and translate to the "3D" circulation, and "inner" routines that contain the actual biogeochemical sources and sinks, and define the biogeochemical

GMDD
8, 1945–2010, 2015

parameters (BGC_MODEL.F, BGC_INI.F). They communicate via common blocks in header files BGC_PARAMS.h and BGC_CONTROL.h.

external_forcing_kiel_biogeochem.c mainly connects the biogeochemical subroutines to the TMM. It also reads the I/O files and runtime parameters. It calls the following subroutines:

- kiel_biogeochem_ini.F carries out some basic initialization, such as setting the time step length, initializing the tracer fields and vertical model structure, as well as some parts of the carbonate system (option -DCARBON, see below). It calls
  - BGC_INI.F, which sets the biogeochemical parameters (e.g., max. growth rate of phytoplankton, etc.) and may call CAR_INI.F to define the parameters for the carbon module (option -DCARBON, see below).
- kiel_biogeochem_model.F maps the 1D tracer fields used by the TMM onto 1D arrays used by the biogeochemical "core"routine BGC_MODEL.F, and back again afterwards. It calls
  - BGC_MODEL.F carries out the actual computation of biogeochemical sources and sinks presented here, including organic matter sinking and remineralization, air–sea gas exchange, computation of carbon chemistry (option -DCARBON, see below). Thus, it is the "heart" of biogeochemistry. This routine requires daily average photosynthetically active solar radiation below sea surface, and daylength. For this, we use a routine insolation.F provided by the MIT (http://mitgcm.org/public/source_code.html), with some minor modifications by us. Any other forcing field for light can be provided.
- kiel_biogeochem_diagnostics.F maps the diagnostic output (production, sedimentation, ... computed in BGC_MODEL onto arrays to be passed to external_forcing_kiel_biogeochem

GMDD
8, 1945–2010, 2015

- `kiel_biogeochem_set_params.F` is a dummy that may serve as future module for changing parameters during optimization.

Communication between the different modules is carried out mainly via header files:

- `BGC_PARAMS.h` is a header file that passes biogeochemical parameters between the different model pieces (from `BGC_INI` to `BGC_MODEL`). It also contains the biogeochemical tracer fields (`bgc_tracer`).
- `BGC_DIAGNOSTICS.h` contains arrays for diagnostic output.
- `BGC_CONTROL.h` is a header file that passes more technical runtime parameters to biogeochemistry, e.g., time step length, and vertical geometry.
- `kiel_biogeochem.h` make subroutines known to `external_forcing_kiel_biogeochem.c`

A rather simple carbon module may be coupled to the P-core via compile option `-DCARBON`. Note that these modules (`CAR_CHEM.F`, `CAR_INI.F`, `CAR_PARAMS.h`) are still somewhat preliminary, and will be presented in a later publication. They are largely based upon the routines developed and provided by MIT (http://mitgcm.org/public/source_code.html).

More documentation, the full model source code, including Makefiles (for compilation with PETSc version 3.3/3.4/3.5 and MPI), runscripts (for CrayXC30; usually just minor changes required for other Linux clusters), model forcing and output from sample runs e.g. of RemHigh with medium sinking speed are available from the author Iris Kriest upon request.

The Supplement related to this article is available online at doi:10.5194/gmdd-8-1945-2015-supplement.

Acknowledgements. This work is a contribution to the DFG-supported project SFB754. Parallel supercomputing resources have been provided by the North-German Supercomputing Alliance (HLRN). The authors wish to acknowledge use of the Ferret program of NOAA's Pacific Marine Environmental Laboratory for analysis and graphics in this paper.

GMDD
8, 1945–2010, 2015

References

Anderson, L.: On the hydrogen and oxygen content of marine phytoplankton, Deep-Sea Res. Pt. I, 42, 1675–1680, 1995. 1959

Anderson, L. and Sarmiento, J.: Redfield ratios of remineralization determined by nutrient data analysis, Global Biogeochem. Cy., 8, 65–80, 1994. 1986

Babbin, A., Keil, R., Devol, A., and Ward, B.: Organic matter stoichiometry, flux, and oxygen control nitrogen loss in the ocean, Science, 344, 406–408, doi:10.1126/science.1248364, 2014. 1969

Bianchi, D., Dunne, J. P., Sarmiento, J. L., and Galbraith, E. D.: Data-based estimates of suboxia, denitrification, and N_2O production in the ocean and their sensitivities to dissolved O_2, Global Biogeochem. Cy., 26, GB2009, doi:10.1029/2011GB004209, 2012. 1962, 1999

Breitbarth, E. and LaRoche, J.: Importance of the diazotrophs as a source of new nitrogen in the ocean, J. Sea Res., 53, 67–91, 2005. 1947, 1952, 1980

Breitbarth, E., Oschlies, A., and LaRoche, J.: Physiological constraints on the global distribution of *Trichodesmium* – effect of temperature on diazotrophy, Biogeosciences, 4, 53–61, doi:10.5194/bg-4-53-2007, 2007. 1947, 1981

Bulow, S., Rich, J., Naik, H., Pratihary, A., and Ward, B.: Denitrification exceeds anammox as a nitrogen loss pathway in the Arabian Sea oxygen minimum zone, Deep-Sea Res. Pt. I, 57, 384–393, doi:10.1016/j.dsr.2009.10.014, 2010. 1948, 1960

Codispoti, L.: An oceanic fixed nitrogen sink exceeding $400\,\mathrm{Tg\,N\,a^{-1}}$ vs the concept of homeostasis in the fixed-nitrogen inventory, Biogeosciences, 4, 233–253, 2007. 1947, 1962

Codispoti, L., Brandes, J., Christensen, J., Devol, A., Naqvi, S., Paerl, H., and Yoshinari, T.: The oceanic fixed nitrogen and nitrous oxide budgets: moving targets as we enter the anthropocene?, Sci. Mar., 65, 85–105, 2001. 1947

Dalsgaard, T., Thamdrup, B., Farias, L., and Revsbech, N.: Anammox and denitrification in the oxygen minimum zone of the eastern South Pacific, Limnol. Oceanogr., 57, 1331–1346, doi:10.4319/lo.2012.57.5.1331, 2012. 1961, 1968, 1969, 1970

Dalsgaard, T., De Brabandere, L., and Hall, P.: Denitrification in the water column of the central Baltic Sea, Geochim. Cosmochim. Ac., 106, 247–260, doi:10.1016/j.gca.2012.12.038, 2013. 1970

De Brabandere, L., Canfield, D., Dalsgaard, T., Friederich, G., Revsbech, N., Ulloa, O., and Thamdrup, B.: Vertical partitioning of nitrogen-loss processes across the oxic-anoxic

GMDD
8, 1945–2010, 2015

interface of an oceanic oxygen minimum zone, Environ. Microbiol., 16, 3041–3054, doi:10.1111/1462-2920.12255, 2013. 1970

Deutsch, C., Sigman, D., Thunell, R., An, A. M., and Haug, G.: Isotopic constraints on glacial/interglacial changes in the oceanic nitrogen budget, Global Biogeochem. Cy., 18, GB4012, doi:10.1029/2003GB002189, 2004. 1962, 1999

Deutsch, C., Sarmiento, J. L., Sigman, D. M., Gruber, N., and Dunne, J. P.: Spatial coupling of nitrogen inputs and losses in ocean, Nature, 445, 163–167, doi:10.1038/nature05392, 2007. 1947, 1963, 1999

DeVries, T., Deutsch, C., Primeau, F., Chang, B., and Devol, A.: Global rates of water-column denitrification derived from nitrogen gas measurements, Nat. Geosci., 5, 547–550, doi:10.1038/NGEO1515, 2012. 1962, 1999

DeVries, T., Deutsch, C., Rafter, P. A., and Primeau, F.: Marine denitrification rates determined from a global 3-dimensional inverse model, Biogeosciences, 10, 2481–2496, doi:10.5194/bg-10-2481-2013, 2013. 1947, 1962, 1999

Dietze, H. and Loeptien, U.: Revisiting "nutrient trapping" in global coupled biogeochemical ocean circulation models, Global Biogeochem. Cy., 27, 265–284, doi:10.1002/gbc.20029, 2013. 1948, 1958, 1967, 1971, 1972

Duteil, O. and Oschlies, A.: Sensitivity of simulated extent and future evolution of marine suboxia to mixing intensity, Geophys. Res. Lett., 38, L06607, doi:10.1029/2011GL046877, 2011. 1948

Duteil, O., Schwarzkopf, F. U., Böning, C. W., and Oschlies, A.: Major role of equatorial current system in setting oxygen levels in the eastern tropical Atlantic Ocean: a high resolution model study, Geophys. Res. Lett., 41, 2033–2040, doi:10.1002/2013GL058888, 2014. 1948

Eugster, O. and Gruber, N.: A probabilistic estimate of global marine N-fixation and denitrification, Global Biogeochem. Cy., 26, GB4013, doi:10.1029/2012GB004300, 2012. 1947, 1948, 1962, 1963, 1999

Evans, G. T. and Parslow, J. S.: A model of annual plankton cycles, Biol. Oceanogr., 3, 327–347, 1985. 1976

Galan, A., Molina, V., Thamdrup, B., Woebken, D., Lavik, G., Kuypers, M., and Ulloa, O.: Anammox bacteria and the anaerobic oxidation of ammonium in the oxygen minimum zone off northern Chile, Deep-Sea Res. Pt. II, 56, 1021–1031, doi:10.1016/j.dsr2.2008.09.016, 2009. 1948, 1961, 1968

GMDD
8, 1945–2010, 2015

Galloway, J. N., Dentener, F. J., Capone, D. G., Boyer, E. W., Howarth, R. W., Seitzinger, S. P., Asner, G. P., Cleveland, C., Green, P., Holland, E., Karl, D. M., Michaels, A. F., Porter, J. H., Townsend, A., and Vörösmarty, C.: Nitrogen cycles: past, present and future, Biogeochemistry, 70, 153–226, doi:10.1007/s10533-004-0370-0, 2004. 1962, 1999

Garcia, H. E., Locarnini, R. A., Boyer, T. P., and Antonov, J. I.: World Ocean Atlas 2005, Vol. 4: Nutrients (phosphate, nitrate, silicate), in: NOAA Atlas NESDIS 64, edited by: Levitus, S., US Government Printing Office, Washington D.C., available at: http://iridl.ldeo.columbia.edu/SOURCES/.NOAA/.NODC/.WOA05/ (last access: 16 May 2008), 2006a. 1953, 2002, 2003, 2007

Garcia, H. E., Locarnini, R. A., Boyer, T. P., and Antonov, J. I.: World Ocean Atlas 2005, Vol. 3: Dissolved Oxygen, Apparent Oxygen Utilization, and Oxygen Saturation, in: NOAA Atlas NESDIS 63, edited by: Levitus, S., US Government Printing Office, Washington D.C., available at: http://iridl.ldeo.columbia.edu/SOURCES/.NOAA/.NODC/.WOA05/ (last access: 16 May 2008), 2006b. 1953, 2002, 2003, 2007

Getzlaff, J. and Dietze, H.: Effects of increased isopycnal diffusivity mimicking the unresolved equatorial intermediate current system in an earth system climate model, Geophys. Res. Lett., 40, 2166–2170, doi:10.1002/grl.50419, 2013. 1948, 1972

Gnanadesikan, A., Bianchi, D., and Pradal, M.-A.: Critical role for mesoscale eddy diffusion in supplying oxygen to hypoxic ocean waters, Geophys. Res. Lett., 40, 5194–5198, doi:10.1002/grl.50998, 2013. 1961

Goebel, N., Edwards, C., Church, M., and Zehr, J.: Modeled contributions of three types of diazotrophs to nitrogen fixation at Station ALOHA, ISME J., 1, 606–619, doi:10.1038/ismej.2007.80, 2007. 1980, 1982

Gruber, N.: The dynamics of the marine nitrogen cycle and its influence on atmospheric CO_2 variations, in: Carbon–Climate Interactions, edited by: Oguz, T. and Follows, M., NATO ASI, John Wiley & Sons Ltd., 2004. 1947

Gruber, N. and Sarmiento, J.: Global patterns of marine nitrogen fixation and denitrification, Global Biogeochem. Cy., 11, 235–266, 1997. 1947, 1962, 1999

Hamersley, M., Lavik, G., Woebken, D., Rattray, J., Lam, P., Hopmans, E., Sinnighe Damste, J., Krüger, S., Graco, M., Gutierrez, D., and Kuypers, M.: Anaerobic ammonium oxidation in the Peruvian oxygen minimum zone, Limnol. Oceanogr., 52, 923–933, 2007. 1961, 1968

Ilyina, T., Six, K., Segschneider, J., Maier-Reimer, E., Li, H., and nez Riboni, I. N.: Global ocean biogeochemistry model HAMOCC: model architecture and performance as component of the

GMDD
8, 1945–2010, 2015

MPI-Earth system model in different CMIP5 experimental realizations, J. Adv. Model. Earth Syst., 5, 1–29, doi:10.1029/2012MS000178, 2013. 1952, 1966
Jensen, M., Petersen, J., Dalsgaard, T., and Thamdrup, B.: Pathways, rates, and regulation of N_2 production in the chemocline of an anoxic basin, Mariager Fjord, Denmark, Mar. Chem., 113, 102–113, doi:10.1016/j.marchem.2009.01.002, 2009. 1951, 1970, 1971, 1988
Jolliff, J., Kindle, J., Shulman, I., Penta, B., Friedrichs, M., Helber, R., and Arnone, R.: Summary diagrams for coupled hydrodynamic-ecosystem model skill assessment, J. Mar. Syst., 76, 64–82, doi:10.1016/j.jmarsys.2008.05.014, 2009. 1958, 1964
Kalvelage, T., Jensen, M. M., Contreras, S., Revsbech, N. P., Lam, P., Guenter, M., LaRoche, J., Lavik, G., and Kuypers, M. M. M.: Oxygen sensitivity of anammox and coupled N-cycle Processes in oxygen minimum zones, PLoS ONE, 6, e29299, doi:10.1371/journal.pone.0029299, 2011. 1949, 1951, 1960, 1961, 1968, 1970, 1983
Kalvelage, T., Lavik, G., Lam, P., Contreras, S., Arteaga, L., Löscher, C., Oschlies, A., Paulmier, A., Stramma, L., and Kuypers, M.: Nitrogen cycling driven by organic matter export in the South Pacific oxygen minimum zone, Nat. Geosci., 6, 228–234, doi:10.1038/NGEO1739, 2013. 1948
Khatiwala, S.: A computational framework for simulation of biogeochemical tracers in the ocean, Global Biogeochem. Cy., 21, GB3001, doi:10.1029/2007GB002923, 2007. 1953
Khatiwala, S., Visbeck, M., and Cane, M. A.: Accelerated simulation of passive tracers in ocean circulation models, Ocean Modell., 9, 51–69, 2005. 1988
Kitajima, S., Furuya, K., Hashihama, F., and Takeda, S.: Latitudinal distribution of diazotrophs and their nitrogen fixation in the tropical and subtropical western North Pacific, Limnol. Oceanogr., 54, 537–547, 2009. 1959, 1960, 1982
Koeve, W. and Kähler, P.: Heterotrophic denitrification vs. autotrophic anammox – quantifying collateral effects on the oceanic carbon cycle, Biogeosciences, 7, 2327–2337, doi:10.5194/bg-7-2327-2010, available at: www.biogeosciences.net/7/2327/2010/, 2010. 1969
Kriest, I. and Oschlies, A.: On the treatment of particulate organic matter sinking in large-scale models of marine biogeochemical cycles, Biogeosciences, 5, 55–72, available at: http://www.biogeosciences.net/5/55/2008/, 2008. 1977
Kriest, I. and Oschlies, A.: Swept under the carpet: organic matter burial decreases global ocean biogeochemical model sensitivity to remineralization length scale, Biogeosciences,

GMDD
8, 1945–2010, 2015

10, 8401–8422, doi:10.5194/bg-10-8401-2013, 2013. 1950, 1953, 1964, 1965, 1978, 1998, 2002, 2008

Kriest, I., Khatiwala, S., and Oschlies, A.: Towards an assessment of simple global marine biogeochemical models of different complexity, Prog. Oceanogr., 86, 337–360, doi:10.1016/j.pocean.2010.05.002, 2010. 1976, 1978

Kriest, I., Oschlies, A., and Khatiwala, S.: Sensitivity analysis of simple global marine biogeochemical models, Global Biogeochem. Cy., 26, GB2029, doi:10.1029/2011GB004072, 2012. 1950, 1953, 1976, 1978

Kuypers, M., Lavik, G., Woebken, D., Schmid, M., Fuchs, B., Amann, R., Jørgensen, B., and Jetten, M.: Massive nitrogen loss from the Benguela upwelling system through anaerobic ammonium oxidation, Proc. Nat. Acad. Sci., 102, 6478–6483, doi:10.1073/pnas.0502088102, 2005. 1948, 1960

Landolfi, A., Dietze, H., Koeve, W., and Oschlies, A.: Overlooked runaway feedback in the marine nitrogen cycle: the vicious cycle, Biogeosciences, 10, 1351–1363, doi:10.5194/bg-10-1351-2013, 2013. 1947, 1949

Letelier, R. and Karl, D.: Role of *Trichodesmium* spp. in the productivity of the subtropical North Pacific Ocean, Mar. Ecol.-Prog. Ser., 133, 263–273, 1996. 1980, 1982

Luo, Y.-W., Doney, S. C., Anderson, L. A., Benavides, M., Berman-Frank, I., Bode, A., Bonnet, S., Boström, K. H., Böttjer, D., Capone, D. G., Carpenter, E. J., Chen, Y. L., Church, M. J., Dore, J. E., Falcón, L. I., Fernández, A., Foster, R. A., Furuya, K., Gómez, F., Gundersen, K., Hynes, A. M., Karl, D. M., Kitajima, S., Langlois, R. J., LaRoche, J., Letelier, R. M., Marañón, E., McGillicuddy Jr., D. J., Moisander, P. H., Moore, C. M., Mouriño-Carballido, B., Mulholland, M. R., Needoba, J. A., Orcutt, K. M., Poulton, A. J., Rahav, E., Raimbault, P., Rees, A. P., Riemann, L., Shiozaki, T., Subramaniam, A., Tyrrell, T., Turk-Kubo, K. A., Varela, M., Villareal, T. A., Webb, E. A., White, A. E., Wu, J., and Zehr, J. P.: Database of diazotrophs in global ocean: abundance, biomass and nitrogen fixation rates, Earth Syst. Sci. Data, 4, 47–73, doi:10.5194/essd-4-47-2012, 2012. 1947, 1960, 1974, 1980, 1982

Mahaffey, C., Michaels, A., and Capone, D.: The conundrum of marine N_2 fixation, Am. J. Sci., 305, 546–595, 2005. 1959

Maier-Reimer, E., Kriest, I., Segschneider, J., and Wetzel, P.: The HAMburg Ocean Carbon Cycle Model HAMOCC 5.1 – Technical Description Release 1.1, Reports on Earth System Science 14, Max-Planck-Institute for Meteorology, Hamburg, available at: http://www.mpimet.

GMDD

8, 1945–2010, 2015

mpg.de/fileadmin/publikationen/erdsystem_14.pdf (last access: 26 September 2005), 2005. 1952

Martin, J. H., Knauer, G. A., Karl, D. M., and Broenkow, W. W.: VERTEX: carbon cycling in the Northeast Pacific, Deep-Sea Res., 34, 267–285, 1987. 1965

Moore, J. K. and Doney, S. C.: Iron availability limits the ocean nitrogen inventory stabilizing feedbacks between marine denitrification and nitrogen fixation, Global Biogeochem. Cy., 21, GB2001, doi:10.1029/2006GB002762, 2007. 1949, 1962, 1966, 1986, 1999

Mulholland, M. R.: The fate of nitrogen fixed by diazotrophs in the ocean, Biogeosciences, 4, 37–51, doi:10.5194/bg-4-37-2007, 2007. 1982

Najjar, R. G., Jin, X., Louanchi, F., Aumont, O., Caldeira, K., Doney, S. C., Dutay, J.-C., Follows, M., Gruber, N., Joos, F., Lindsay, K., Maier-Reimer, E., Matear, R., Matsumoto, K., Monfray, P., Mouchet, A., Orr, J. C., Plattner, G.-K., Sarmiento, J. L., Schlitzer, R., Slater, R. D., Weirig, M.-F., Yamanaka, Y., and Yool, A.: Impact of circulation on export production, dissolved organic matter and dissolved oxygen in the ocean: results from phase II of the Ocean Carbon-Cycle Model Intercomparison Project (OCMIP-2), Global Biogeochem. Cy., 21, GB3007, doi:10.1029/2006GB002857, 2007. 1986

Oschlies, A., Schulz, K., Riebesell, U., and Schmittner, A.: Simulated 21st century's increase in oceanic suboxia by CO_2-enhanced biotic carbon export, Global Biogeochem. Cy., 22, GB4008, doi:10.1029/2007GB003147, 2008. 1962, 1999

Paulmier, A., Kriest, I., and Oschlies, A.: Stoichiometries of remineralisation and denitrification in global biogeochemical ocean models, Biogeosciences, 6, 923–935, doi:10.5194/bg-6-923-2009, 2009. 1950, 1951, 1968, 1969, 1986, 1987

Richards, F.: Anoxic basins and fjords, in: Chemical Oceanography, vol. 1, chap. 13, edited by: Riley, J. and Skirrow, G., Academic Press, New York, 611–645, 1965. 1969, 1987

Schmittner, A., Oschlies, A., Matthews, H. D., and Galbraith, E. D.: Future changes in climate, ocean circulation, ecosystems, and biogeochemical cycling simulated for a business-as-usual CO_2 emission scenario until year 4000 AD, Global Biogeochem. Cy., 22, GB1013, doi:10.1029/2007GB002953, 2008. 1966, 1976

Somes, C. J., Oschlies, A., and Schmittner, A.: Isotopic constraints on the pre-industrial oceanic nitrogen budget, Biogeosciences, 10, 5889–5910, doi:10.5194/bg-10-5889-2013, 2013. 1947, 1963, 1999

GMDD
8, 1945–2010, 2015

Staal, M., te Lintel Hekkert, S., Brummer, G., Veldhuis, M., Sikkens, C., Persijn, S., and Stal, L.: Nitrogen fixation along a north-south transect in the eastern Atlantic Ocean, Limnol. Oceanogr., 52, 1305–1316, 2007. 1959, 1960, 1982

Stammer, D., Ueyoshi, K., Köhl, A., Large, W. G., Josey, S. A., and Wunsch, C.: Estimating air–sea fluxes of heat, freshwater, and momentum through global ocean data assimilation, J. Geophys. Res., 109, C05023, doi:10.1029/2003JC002082, 2004. 1953, 1971

Taylor, K.: Summarizing multiple aspects of model performance in a single diagram, J. Geophys. Res., 106, 7183–7192, 2001. 1957, 1958, 2003

Thamdrup, B., Dalsgaard, T., Jensen, M., Ulloa, O., Faria, L., and Escribano, R.: Anaerobic ammonium oxidation in the oxygen-deficient waters off northern Chile, Limnol. Oceanogr., 51, 2145–2156, 2006. 1968

Ward, B.: How nitrogen is lost, Science, 341, 352–353, doi:10.1126/science.1240314, 2013. 1969

Ward, B., Tuit, C., Jayakumar, A., Rich, J., Moffett, J., and Naqvi, S.: Organic carbon, and not copper, controls denitrification in oxygen minimum zones of the ocean, Deep-Sea Res. Pt. I, 55, 1672–1683, doi:10.1016/j.dsr.2008.07.005, 2008. 1948

Ward, B., Devol, A., Rich, J., Chang, B., Bulow, S., Naik, H., Pratihary, A., and Jayakumar, A.: Denitrification as the dominant nitrogen loss process in the Arabian Sea, Nature, 461, 78–82, doi:10.1038/nature08276, 2009. 1948, 1960

GMDD
8, 1945–2010, 2015

Table 1. Model parameters for aerobic and anaerobic remineralization and nitrogen fixation in different experimental setups of model MOPS: "REF": Reference experiment; "NFixNoTemp": no temperature dependence of nitrogen fixation; "NFixStoich": changed stoichiometry of nitrogen fixation; "DenHigh": increased nitrate affinity of denitrification; "RemHigh": increased oxidant (nitrate and oxygen) affinity of total (oxic and suboxic) remineralisation. All other models parameters are as in Kriest and Oschlies (2013), experiment BUR.

Name	REF	NFixNoTemp	NFixStoich	DenHigh	RemHigh	unit
d	16	16	16	16	16	mmol N : mmol P
$R_{-O_2:P}$	170	170	170	170	170	mmol O_2 : mmol P
$\min_{O_2}$	4	4	4	4	1	mmol O_2 m^{-3}
K_{O_2}	8	8	8	8	2	mmol O_2 m^{-3}
$R_{-NO_3:P}$	120	120	120	120	120	mmol NO_3 : mmol P
$\min_{NO_3}$	4	4	4	4	4	mmol N m^{-3}
K_{NO_3}	32	32	32	8	8	mmol N m^{-3}
μ^*_{NFix}	2	2	2	2	2	nmol N L^{-1} d^{-1}
	yes	no	yes	yes	yes	
d^*	16	16	14.28	16	16	mmol N : mmol P

GMDD
8, 1945–2010, 2015

Table 2. Global fixed nitrogen fluxes [Tg y^{-1}] from model experiments, and results from other model studies and biogeochemical observations. "gain" refers to pelagic nitrogen fixation, while "loss" refers to nitrogen loss through pelagic denitrification. For each model type model we give the results of the reference run, and in brackets the range encompassed by experiments s2–s3 with different particle sinking speeds.

Source	pelagic loss	gain	comments
Gruber and Sarmiento (1997)	80	110	observations of N^*
Galloway et al. (2004)	81	85	direct measurements, geochemical estimates
Deutsch et al. (2004)	70	260	N^*, isotopes, box model
Moore and Doney (2007)	65 (0–189)	58 (0–133)	global BGC OGCM
Deutsch et al. (2007)		137 (130–158)	global BGC OGCM, observed nutrients
Oschlies et al. (2008)		140	global BGC OGCM
Bianchi et al. (2012)	70 ±50		observed oxygen, production, export model
Eugster and Gruber (2012)	52 (39–66)	131 (94–175)	box model, observed N^* and ^{15}N
DeVries et al. (2012)	66 ±6		inv. global model, obs. excess N_2, observed production or nutrients
DeVries et al. (2013)	60 (50–77)		inv. global model, obs. N^* and ^{15}N
Somes et al. (2013)	76 (65–80)	225 (195–350)	global model inc. nitrogen isotopes
this study: REF	59 (27–87)		reference run
this study: NFixStoich	59 (27–87)		N : P=14.28 for nitrogen fixation
this study: NFixNoTemp	65 (29–97)		T-independent nitrogen fixation
this study: DenHigh	84 (41–117)		high nitrate affinity
this study: RemHigh	71 (29–105)		high nitrate and oxygen affinity

GMDD
8, 1945–2010, 2015

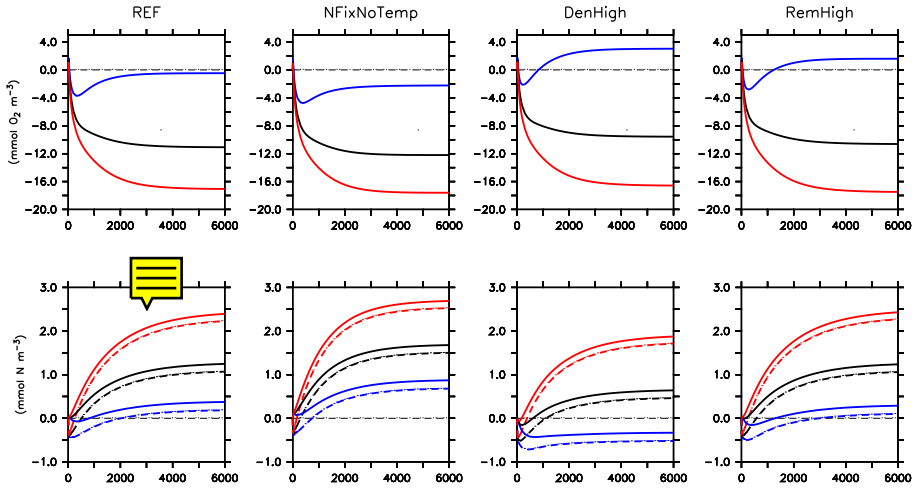

Figure 1. Transient behavior of global average oxygen (top), nitrate (bottom, dashed lines) and fixed nitrogen (bottom, straight lines) in different setups of model MOPS, plotted as deviation from initial average ($\bar{x}(t) - \bar{x}(0)$, where $\bar{x}$ is either global average oxygen or nitrate). Average tracers are calculated from snapshots of day 360 every 10th year within the first 200 years, and every 100th year thereafter. Line colours denote different sinking speeds: Red – "fast", black: "medium", blue – "slow". Model identifier is shown on top of each column. For better visibility, we only show the first 6000 years of simulation.

GMDD
8, 1945–2010, 2015

MOPS-1.0: modelling the regulation of the oceanic nitrogen budget

I. Kriest and A. Oschlies

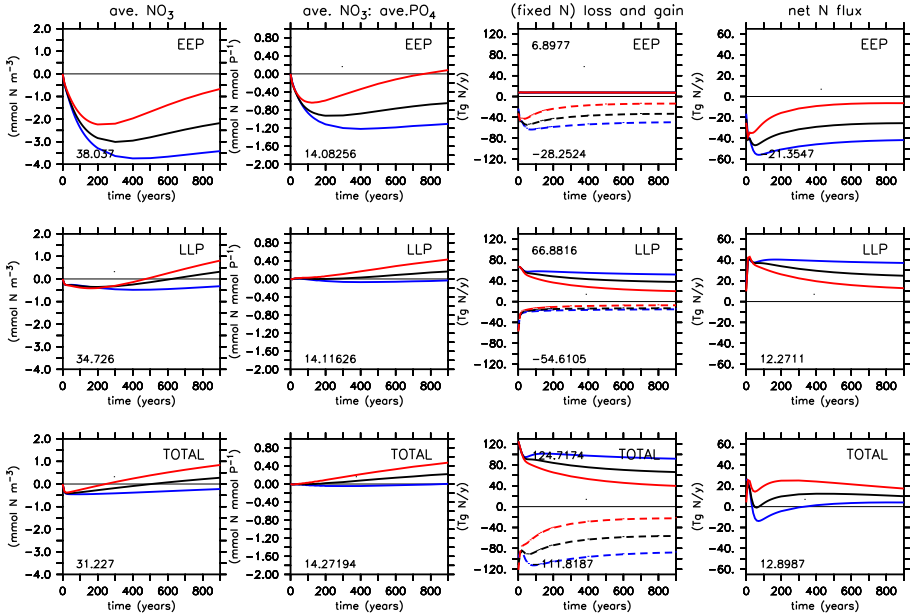

Figure 2. From left to right: transient behavior of average nitrate, average nitrate : average phosphate ratio, fixed nitrogen fluxes, and net fixed nitrogen flux in the Eastern Equatorial Pacific ("EEP", east of 140° W, ±10° latitude; top), surrounding low-latitude Pacific region ("LLP", ±40° latitude; middle), and for the global ocean (bottom) in reference setup REF. Diagnostics are plotted as deviation from initial average ($\bar{x}(t) - \bar{x}(0)$, where $\bar{x}$ is global average diagnostic). Average tracers (fluxes) are calculated from snapshots of day 360 (concentrations) or annual integrals (fluxes) every 10th year within the first 200 years, and every 100th year thereafter. Line colours denote different sinking speeds: Red – "fast", black: "medium", blue – "slow". Dashed lines in plots for fixed N loss and gain denote the losses (denitrification), straight lines the gains (nitrogen fixation).

GMDD
8, 1945–2010, 2015

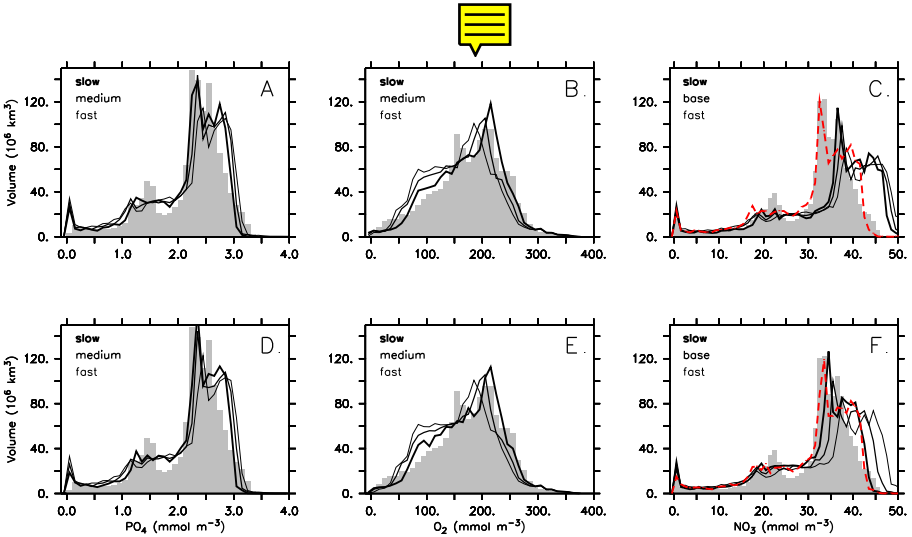

Figure 3. Volume distributions of global phosphate (panels **a**, **d**), oxygen (panels **b**, **e**) and nitrate (panels **c**, **f**) for model BUR of Kriest and Oschlies (2013, upper panels **a**–**c**), and experiment REF of MOPS (lower panels **d**–**f**). Grey bars denote the corresponding observations (Garcia et al., 2006a, b). Lines thickness denotes different sinking speeds. Thick: slow sinking. Medium: medium sinking. Thin: fast sinking. Nitrate for model BUR (without nitrogen cycle) has been calculated from phosphate ×16 addition, we present nitrate calculated from phosphate ×14.28 for the "slow" sinking scenario as thick dashed red lines.

GMDD
8, 1945–2010, 2015

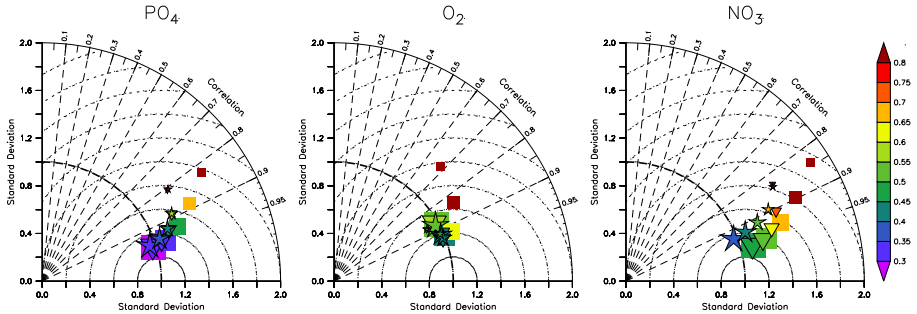

Figure 4. Taylor diagrams showing comparison of simulated phosphate (left), oxygen (middle), and nitrate (right) to observations (Garcia et al., 2006a, b). Symbols indicate model setups: Squares: CTL. Inverted traingles: BUR. Stars: REF. Symbol size indicates model sinking speed, with size increasing from $b = 0.429$ (fast) to $b = 1.287$ (slow). x and y axis denotes SD normalized by observed global SD of each tracer. Radial dashed lines denote the correlation coefficient. Dotted lines centric lines denote the centric (unbiased) RMSE (E' in Taylor, 2001). Colours denote total RMSE (E in Taylor, 2001), normalized by observed SD.

GMDD
8, 1945–2010, 2015

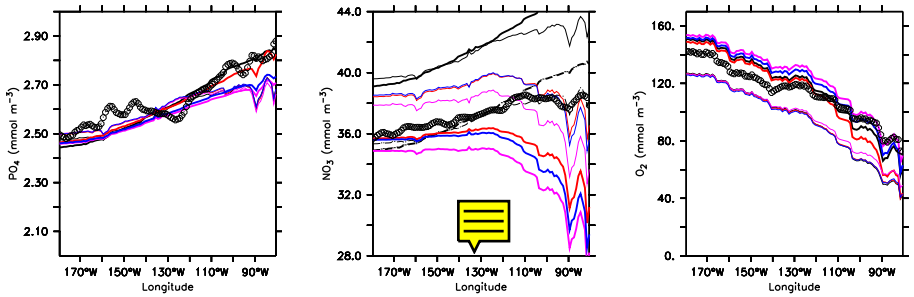

Figure 5. Phosphate (left), nitrate (middle) and oxygen (right) averaged over ±5° and 0–6500 m, and plotted from 180–80° W, for different models (lines) and observations (circles). Black: model BUR (without nitrogen); nitrate is calculated from 16× phosphate (i.e. from the stoichiometry prescribed by the model; straight lines) as well as from 14.28× phosphate (i.e. from the global observed ratio; dashed lines). Red: MOPS, setup REF, Pink: MOPS, setup DenHigh, Blue: MOPS, setup RemHigh. Thin lines denote model experiments with fast sinking speed, thick lines model experiments with slow sinking speed. Note that model axes for phosphate, nitrate and oxygen scale in a ratio of 1 : 16 : 170 (i.e., according to aerobic stoichiometry).

GMDD
8, 1945–2010, 2015

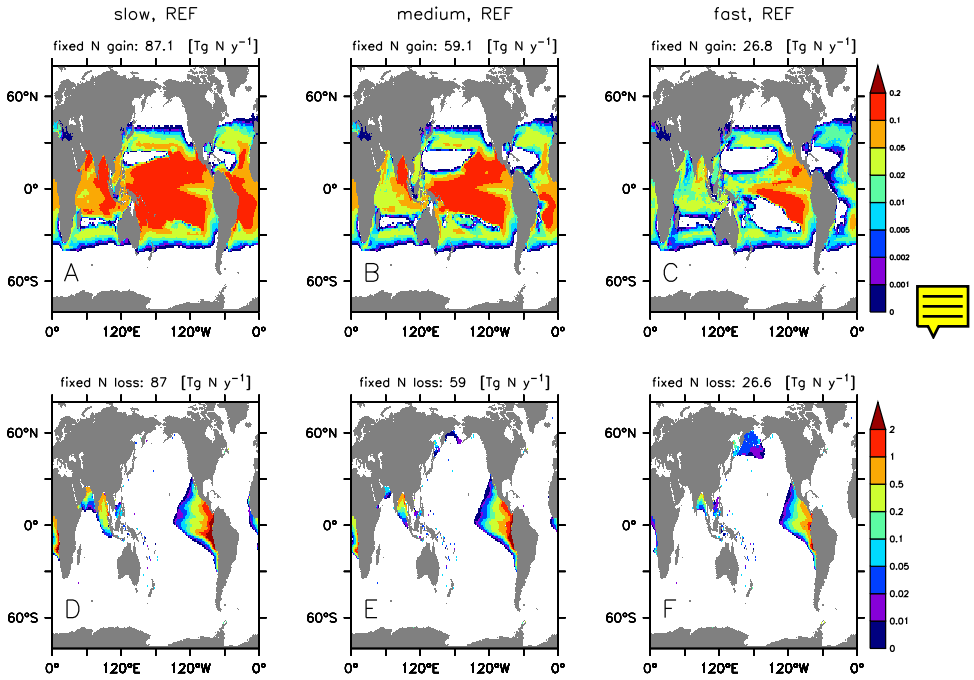

Figure 6. Vertically integrated nitrogen fixation (mmol m^{-2} d^{-1}, panels **a**–**c**), and vertically integrated denitrification (mmol m^{-2} d^{-1}, panels **d**–**f**), for reference setup REF with three different particle sinking speeds "slow" (panels **a**, **d**), "medium" (panels **b**, **e**) and "fast" (panels **c**, **f**). Note non-linear colour scales. Numbers on top of each panel give global integrated flux of year 9001.

GMDD
8, 1945–2010, 2015

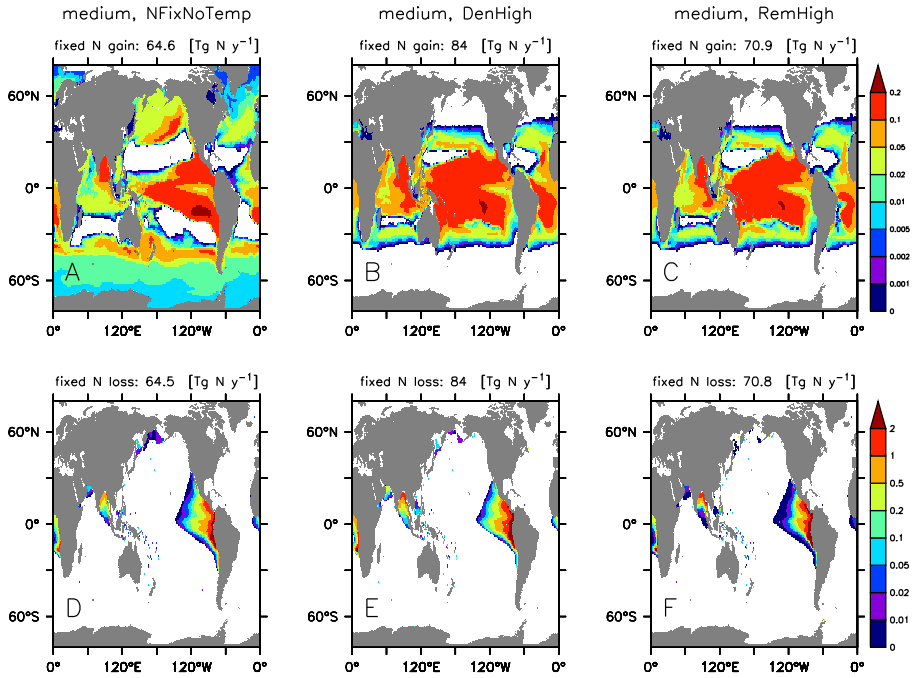

Figure 7. As Fig. 6, but for "medium" configuration of NFixNoTemp (no temperature dependence of nitrogen fixation, panels **a**, **d**), model setup DenHigh (high nitrate affinity of denitrification, panels **b**, **e**) and model setup RemHigh (high oxidant affinity of denitrification and aerobic remineralization, panels **c**, **f**).

GMDD
8, 1945–2010, 2015

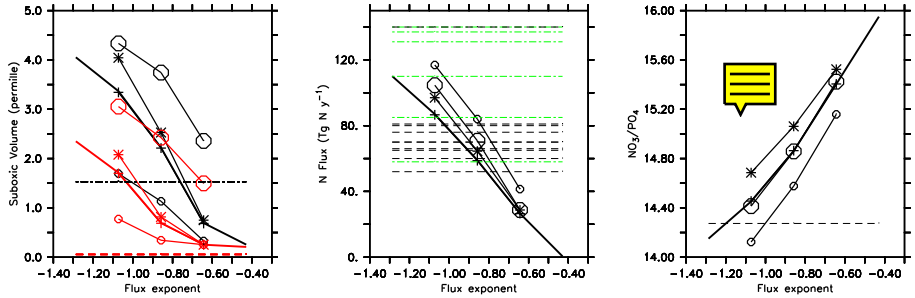

Figure 8. Global diagnostics for different experiments with model MOPS, plotted vs. particle flux exponent (sinking speed increasing from left to right) Left: suboxic volume (as permille of total ocean volume) for different model experiments and according to different criteria (black lines: volume with oxygen $< 8\,\mathrm{mmol\,O_2\,m^{-3}}$, red lines: volume with oygen $< 4\,\mathrm{mmol\,O_2\,m^{-3}}$). Mid: global nitrogen loss (models and observations, black) and nitrogen fixation (observations, green). Note that in the models, due to their intrinsic assumptions pelagic nitrogen loss equates with nitrogen gain through nitrogen fixation. Right: global nitrate : phosphate ratio of different models. Straight lines denote model results. Thick line: setup REF. Thin line with pluses: setup NFixStoich. Thin line with stars: setup NFixNoTemp. Thin line with small circles: setup DenHigh. Thin line with large circles: setup RemHigh. Horizontal dashed lines depict observations. Left and right: observations according to Garcia et al. (2006a, b). Mid: observations for pelagic denitrification (black) and nitrogen fixation (green) from sources listed in Table 2.

GMDD
8, 1945–2010, 2015

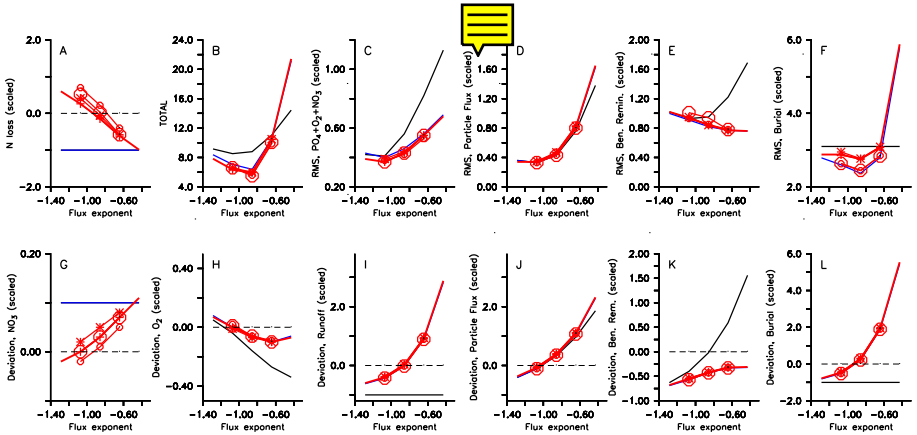

Figure 9. Normalized (scaled) misfit for different models plotted vs. particle flux exponent (sinking speed increasing from left to right). Normalization has been carried out using globally integrated fluxes and inventories, or average concentrations. See auxiliary table "fullmetrics.txt" in the Supplement for norms and numerical values of tracer misfits. **(a)** normalized deviation between simulated and observed global nitrogen loss via pelagic denitrification. **(c)** sum of normalized misfit (root-mean-square-error, RMS) for phosphate, oxygen and nitrate; **(d–f)** normalized RMS for particle flux in 2000 m **(d)**, benthic remineralization **(e)**, benthic burial **(f)**. **(g–l)** normalized deviation between simulated and observed global inventory of nitrate **(g)**, oxygen **(h)**, between global global river runoff of phosphate **(i)**, organic particles flux **(j)**, benthic remineralization **(k)**, and benthic burial **(l)**. **(b)** finally shows the sum over all panels **(a)** and **(c)** to **(l)**. Line colours and symbols indicate model setup. Black and blue: models "CTL" and "BUR" of Kriest and Oschlies (2013), without and with burial at the sea floor, respectively. Red: model MOPS with nitrogen cycle. Straight red: "REF"; stars: "NFixNoTemp"; large plus: "NFixStoich"; small circles: "DenHigh"; large circles: "RemHigh".

GMDD
8, 1945–2010, 2015

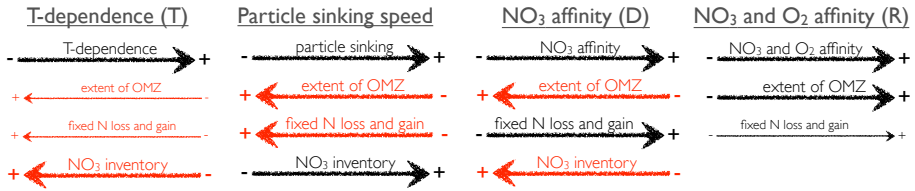

Figure 10. Sketch illustrating the effects of parameter variations on size of the OMZ, nitrogen loss and gain, and global nitrate inventory, for setup NFixNoTemp (left), particle sinking speed (second from left), setup DenHigh (second from right) and setup RemHigh (right). A red arrow denotes a model response that is opposed to the change in parameter. See text for further explanation.

GMDD
8, 1945–2010, 2015

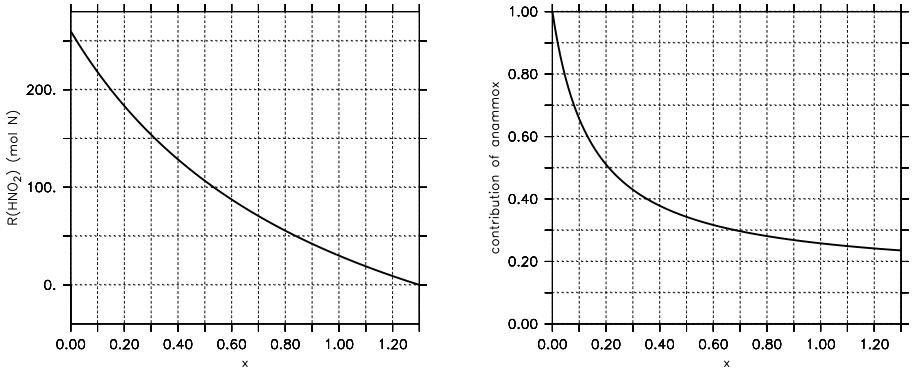

Figure 11. Nitrite surplus per mole of organic phosphorus remineralized (left), and contribution of anammox to fixed nitrogen loss (right) plotted vs. x, the ratio of nitrite reduction rate to nitrate reduction rate for denitrification combined with oxidation of ammonium by anammox. See text for further details.

GMDD
8, 1945–2010, 2015